AD-A155 587 EARLY TIME COUPLING STUDIES USING A 1D HYBRID CODE(U) 1/1
NAVAL RESEARCH LAB WASHINGTON DC C GOODRICH ET AL.
29 MAR 85 NRL-MR-5553

UNCLASSIFIED F/G 18/3 NL

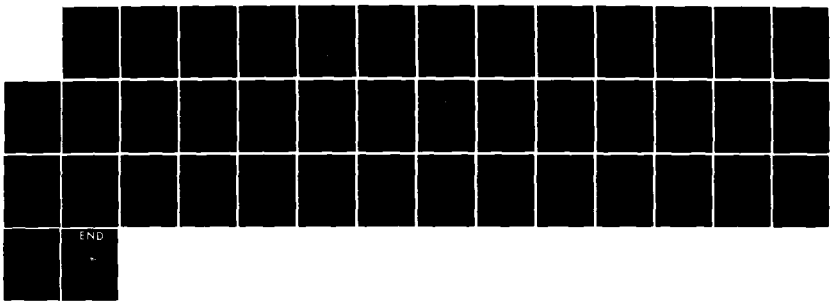

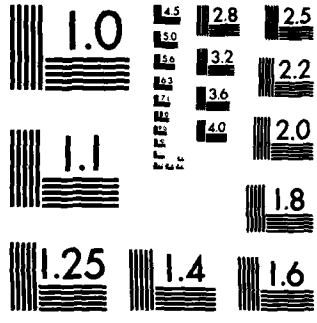

MICROCOPY RESOLUTION TEST CHART
NATIONAL BUREAU OF STANDARDS-1963-A

(2)

NRL Memorandum Report 5553

AD-A155 587

Early Time Coupling Studies Using a 1D Hybrid Code

C. GOODRICH AND K. PAPADOPOULOS

Science Applications International Corporation
McLean, VA 22102

J. D. HUBA

Geophysical and Plasma Dynamics Branch
Plasma Physics Division

May 29, 1985

This work was sponsored by the Defense Nuclear Agency under Subtask S99QMXBC, work unit 00129 and work unit title "Early Time Dynamics."

NAVAL RESEARCH LABORATORY
Washington, D.C.

SECURITY CLASSIFICATION OF THIS PAGE

REPORT DOCUMENTATION PAGE

1a REPORT SECURITY CLASSIFICATION UNCLASSIFIED	1b RESTRICTIVE MARKINGS
2a SECURITY CLASSIFICATION AUTHORITY	3 DISTRIBUTION/AVAILABILITY OF REPORT Approved for public release; distribution unlimited.
2b DECLASSIFICATION/DOWNGRADING SCHEDULE	
4 PERFORMING ORGANIZATION REPORT NUMBER(S) NRL Memorandum Report 5553	5 MONITORING ORGANIZATION REPORT NUMBER(S)
6a NAME OF PERFORMING ORGANIZATION Naval Research Laboratory	6b OFFICE SYMBOL (If applicable) Code 4780
6c ADDRESS (City, State, and ZIP Code) Washington, DC 20375-5000	7b ADDRESS (City, State, and ZIP Code)
8a NAME OF FUNDING/SPONSORING ORGANIZATION Defense Nuclear Agency	8b OFFICE SYMBOL (If applicable) RAAE
8c ADDRESS (City, State, and ZIP Code) Washington, DC 20305	9 PROCUREMENT INSTRUMENT IDENTIFICATION NUMBER
	10 SOURCE OF FUNDING NUMBERS PROGRAM ELEMENT NO: 62715H; PROJECT NO:; TASK NO:; WORK UNIT ACCESSION NO: DN380-296

11 TITLE (Include Security Classification)
Early Time Coupling Studies Using a 1D Hybrid Code

12 PERSONAL AUTHOR(S)
Goodrich, C.,* Papadopoulos, K.,* and Huba, J.

13a TYPE OF REPORT	13b TIME COVERED	14 DATE OF REPORT (Year, Month, Day)	15 PAGE COUNT
Interim	FROM 10/84 TO 10/85	1985 May 29	42

16 SUPPLEMENTARY NOTATION
*Science Applications International Corporation, McLean, VA 22102 (Continues)

17 COSATI CODES			18 SUBJECT TERMS (Continue on reverse if necessary and identify by block number)
FIELD	GROUP	SUB-GROUP	Early time coupling, Ion-ion interactions, 1D Hybrid simulations, Ion energization,

19 ABSTRACT (Continue on reverse if necessary and identify by block number)

The results of simulations of very early time HANE processes (i.e., $t < \Omega_i^{-1}$) using a 1D hybrid code are presented. The purpose of this work is to elucidate important physical phenomena which occur rather than to perform actual early time simulations of a HANE. The focus of this study is primarily on coupling mechanisms. We find that there is no "single" coupling mechanism but that several mechanisms can be effective at various times throughout the debris expansion phase: turbulent coupling, laminar pick-up, and Larmor coupling. Another important result of this study is the generation of very energetic ions. This is caused by the laminar electric field at the leading edge of the magnetic pulse. A fraction of the debris ions can be accelerated up to roughly three times the initial debris expansion velocity (i.e., $V_M \sim 3V_d$). It is well-known that the initial formation of ion debris patches occurs on a time scale faster than that calculated from the initial expansion velocity. Thus, the observation of accelerated debris ions in the simulations is consistent with HANE data.

Keywords:

20 DISTRIBUTION/AVAILABILITY OF ABSTRACT	21 ABSTRACT SECURITY CLASSIFICATION
☒ UNCLASSIFIED/UNLIMITED ☐ SAME AS RPT ☐ DTIC USERS	UNCLASSIFIED
22a NAME OF RESPONSIBLE INDIVIDUAL J. D. Huba	22b TELEPHONE (Include Area Code) (202) 767-3630
	22c OFFICE SYMBOL Code 4780

DD FORM 1473, 84 MAR 83 APR edition may be used until exhausted
All other editions are obsolete

SECURITY CLASSIFICATION OF THIS PAGE

16. SUPPLEMENTARY NOTATION (Continued)

This work was sponsored by the Defense Nuclear Agency under Subtask S99QMXBC, work unit 00129 and work unit title "Early Time Dynamics."

CONTENTS

EARLY TIME COUPLING STUDIES USING A 1D HYBRID CODE

I. INTRODUCTION

The understanding of atmospheric effects generated by a HANE is of vital importance to DNA. It is well known that HANE's cause severe disturbances in the atmosphere and ionosphere which impact C^3I systems. In particular, long lasting, large scale ionization irregularities degrade radar and communications signals. To develop predictive capability for such HANE effects, DNA sponsored a major research effort at NRL leading to theoretical and computational models of HANE. Significant progress was made in this area during the past decade leading to the development of sophisticated multifluid codes which incorporate in a self consistent manner anomalous transport due to instabilities. Recent advances in both plasma theory and numerical techniques allow us today to produce substantially more refined and accurate models of the early time HANE phenomenology. These advances indicate the need for a better incorporation of kinetic effects due to strong deviations of the particle distributions from Maxwellian. The new codes allow us to compute the laminar and turbulent dynamic ion response over long time and space scales and for a mixture of ionized species. In this way laminar, electrostatic, Larmor and turbulent coupling processes can be followed dynamically and their relative strength and dynamic interplay can be assessed. This paper is the first to describe this series of investigations, focuses on a particular process, early time debris-air coupling, and stresses quantitative understanding of the underlying physics.

Early time coupling had been a controversial subject in the DNA HANE community in the 1970's. Two "opposing" views were maintained: NRL, LASL and ARA advocated short-range coupling associated with plasma turbulence, while MRC argued for "Larmor coupling" associated with the ion gyration in the ambient magnetic field. To a certain extent, the issue was not whether or not these coupling mechanisms worked, but which mechanism was dominant. The turbulent coupling process developed at NRL was studied by incorporating theoretical estimates of anomalous transport coefficients in a 1D multi-fluid code. Although this procedure yielded results consistent

Manuscript approved February 14, 1985.

with HANE data and provided strong support for turbulent coupling, it was not a self-consistent technique. Moreover, it was not capable of handling kinetic effects such as caused by reflected ions; such reflected ions are known to occur in high Mach number shocks. The present study, using a 1D hybrid code, overcomes these deficiencies. Namely, it allows instabilities to be excited which affect the plasma evolution in a self-consistent manner, i.e., no model anomalous transport coefficients are used, and reflected ions are permitted. Furthermore, the 1D hybrid code inherently includes "Larmor coupling" so that a direct comparison of the relevant importance and interplay of the coupling mechanisms can be made.

The organization of the paper is as follows. In the next section we present an overview of the basic physical processes occurring as debris streams through the air. In Section III we present results of two simulations which demonstrate the various aspects of coupling. Finally, in the last section we summarize our results and discuss their implications to HANE phenomenology.

II. OVERVIEW OF PHYSICAL PROCESSES

The evolution of the debris-air plasma is characterized by three temporal stages: (1) magnetic field compression; (2) piston formation; and (3) shock formation and evolution. The bulk of this paper describes in detail piston dynamics; for completeness we briefly discuss the other two stages.

In the initial stage, the debris streams outward from the burst point and picks up air electrons which merge with the debris electrons to form a single electron distribution. The compression of the air electrons leads to a compression of the magnetic field since the air electrons are "tied" to the field lines due to the low value of resistivity. This is the first stage of the debris-air interaction and has been well-documented theoretically (Longmire, 1963; Sloan, 1970; Lampe and Hernandez, 1972), numerically (Clark et al., 1974), and experimentally (Ripin et al., 1984).

The next stage involves the dynamics of piston formation and will be discussed in detail in the following section. Briefly, this stage is dominated by the interaction of the two ion streams, i.e., the debris ions and the air ions. It is this phase where various coupling mechanisms

become apparent. The debris ions slow down, while the air ions are picked up; there is momentum exchange between the ion species. There is also a conversion of the directed kinetic energy of the debris to thermal energy of both ions and electrons, i.e., heating and acceleration occurs. And finally, an electrostatic potential forms at the leading edge of the magnetic field compression which causes some debris ions to be accelerated ahead of the magnetic piston and some air ions to be reflected. This final point, although well-known, can be very important to the formation of debris patches in the conjugate regions since it results in very high velocity ions.

Lastly, the final stage involves the formation of a shock wave which "runs" ahead of the piston. We do not describe this phase in detail in this paper, but do show that a minimum time is required for high Mach number shock formation. This minimum time is basically the time needed for the shock to "run" ahead of the accelerated debris or reflected air ions.

III. SIMULATIONS AND RESULTS

Prior to discussing the details of the simulations, we present a simple model equation that elucidates the various coupling mechanisms to be studied. Moreover, it highlights the distinction between previous models (e.g., KLYSMA) and the present work. We consider the following momentum equation in the x direction for an air ion (i.e., radial direction perpendicular to the ambient magnetic field $\underline{B} = B\hat{e}_z$).

$$\frac{dV_{ax}}{dt} = \frac{eE_x}{m_a} + \Omega_a V_{ay} - \nu^*(V_{ax} - V_d) \qquad (1)$$

where the subscript a refers to air, $\Omega_a = Z_a eB/m_a c$, ν^* is an anomalous ion-ion collision frequency, $\underset{\sim}{V}_d = V_d \hat{e}_x$ is the streaming debris velocity, e is the charge, m is the mass, and Z is the charge state. The first term on the RHS of (1) arises from a laminar electric field usually associated with the leading edge of the magnetic compression. It acts to accelerate debris ions and to reflect air ions. The second term in (1) is the magnetic force which is associated with Larmor coupling. The final term in (1) corresponds to turbulent "pick up" of the air and arises because of plasma instabilities. For plasma turbulence such that $\nu^* > \Omega_i$ it is clear that turbulent coupling can dominate over Larmor coupling.

Notice that the force $\Omega_a V_{ay}$ associated with Larmor coupling is proportional to the value of V_{ay} which, before any form of coupling occurs, is $V_{ax} = V_{ay} = 0$. Therefore the laminar force eE_x/m_a and the turbulent force $\nu^*|V_{ax} - V_d| \sim \nu^* V_d$ will dominate initially even for $\nu^* \ll \Omega_a$ (i.e., as long as $\nu^* > \Omega_a(V_{ay}/V_d)$). The time evolution of V_{ay} will be given by

$$\frac{dV_{ay}}{dt} = \frac{eE_y}{m_a} = \frac{eV_d B}{m_a c} = \Omega_a V_d \tag{2}$$

In deriving eq. (1a) we assumed an infinitely conducting ($\eta \to 0$), low β ($\beta \ll 1$) situation so that $E_y = V_d B/c$. From eqs. (1) and (2) it is obvious that the time scale for significant Larmor coupling is $\Omega_a t > 1$, i.e., the value of V_{ay} should approach V_d. At earlier times the laminar and turbulent forces will dominate. The turbulent forces will also dominate even at $t \gg \Omega_a^{-1}$ as long $\nu^* > \Omega_a |V_{ax} - V_d|/V_d$. Another important point follows from (1) and (2) if we neglect the laminar and turbulent forces. If L is the size of magnetic field compression then as long as $V_{ax} < V_d$ the maximum value of V_{ay} will be $V_{ay} = \Omega_a L$. As mentioned previously the Larmor momentum coupling force in the x direction becomes significant if $V_{ay} = \Omega_a L$. Therefore for effective Larmor coupling $L > V_d/\Omega_a$. Namely, an extremely broad magnetic field profile will be required. We will further comment on this point later on.

In previous work, theoretical estimates of ν^* were incorporated in a multi-fluid code (KLYSMA) which solved momentum equations similar to (1) and (2) (Clark et al., 1974). However, the turbulent interaction involves ions interacting with fluctuating electric fields, i.e., $\nu^* = \nu^*(\delta E)$. The present simulations incorporate such effects self-consistently. The air momentum equation solved, analogous to (1), is

$$\frac{dV_{ax}}{dt} = \frac{e}{m_a}\left(E_x + \delta E_x\right) + \Omega_a V_{ay} \tag{3}$$

where δE_x is self consistently generated because of plasma instabilities (e.g., ion-ion streaming instability (Papadopoulos et al., 1971) and is allowed to act directly on the ion motion, rather than through a model equation such as (1). Given this background, we now present the simulation results.

The simulations were performed using a one dimensional quasi-neutral hybrid code (Chodura, 1975; Winske and Leroy, 1984) whose description is given in Appendix I. The code incorporates ion kinetic effects by following the trajectories of "superparticles", numerically representing many actual ions, in 3 dimensions in velocity space and one dimension in configuration space. The electrons are approximated as a massless fluid described by momentum and energy transport equations; the electron pressure is assumed to be isotropic. These equations, with Maxwell's equations, are solved on a one dimensional spatial grid using moments calculated from the ion distributions. Anomalous resistivity, resulting in magnetic field diffusion and electron ohmic heating, is included as a parameter in the equations with a value consistent with that expected from current driven cross-field instabilities.

The boundary conditions in the code correspond to the conditions we expect at early times. A dense ion beam is injected continuously into the simulation box which is initially filled with a tenuous stationary plasma. In our present results both ion populations are H^+, but other ion species can be easily considered and will be presented elsewhere. We set up a finite width magnetic field compression within the leading edge of the ion beam. This represents the field compression expected from the cross-field beam motion which, because of finite resistivity, will diffuse into the beam. The width of the compression has been varied to study various physical phenomena. The magnetic field is held fixed at the edges of the simulation box.

We present below the results of two simulations selected to illustrate the underlying physical coupling processes. The initial state is typical of the piston formation stage. It is shown in Fig. 1a, for the case of $M_A = V_d/V_a = 4$, where V_A is defined on the basis of the ambient (i.e., upstream) parameters. A magnetic pulse consistent with B/n = constant is introduced at the left hand boundary. In this paper we do not study the formation of the pulse but assume its nature in accordance with previous work mentioned in Section II, and its width L to illustrate the important physics. In the figures the velocity is in terms of the upstream value of V_A and of time in terms of the upstream value of Ω_a^{-1}. The units of length are in terms of the ion cyclotron value computed for air with velocity V_d

but with the value of the downstream (i.e., compressed) magnetic field. This representation has been selected for clarity of the underlying physics. We consider (1) a "broad" $L_B = 2R_i$ (R_i in upstream values) pulse with $M_A = 4$ and $n_\alpha/n_a = 16$ and (2) a "narrow" $L_B =$ pulse with $M_A = 8$ and $n_\alpha/n_a = 64$. Here V_d, n_d are the debris velocity and density, n_a the air density and V_A is defined on the basis of the upstream conditions.

A. Broad Pulse $(L_B \approx 2r_{Li})$

This simulation is initialized with a magnetic pulse width $L_B \sim 2r_{Li}$ $V_d/V_A = 4$ and $n_d/n_a = 16$. We show a series of results for this run in Fig. 1. Figure 1 displays four important quantities versus distance. The bottom curve represents the magnetic field magnitude, the middle curve (or "dots") represent particle velocities of the debris and air ions (the debris ions have $V_d \sim 4V_A$ while the air ions have $V_d \sim 0$), and the top curve represents the electric field in the x direction. Figure 1a is at $t = 0.0059\ \Omega_i^{-1}$ where Ω_i is based on the upstream value of $\underset{\sim}{B}$. Note the broad pulse in $\underset{\sim}{B}$ with sharp gradients at the leading and trailing edges. Associated with these gradients are strong laminar electric fields at these edges as shown in the top portion of Fig. 1a. These fields strongly affect the ions. Note in the middle panel that some debris ions are being accelerated ahead of the $\underset{\sim}{B}$ pulse, and air ions are being picked up in a reflection process.

Figure 1b depicts the system at $t = 0.0386\ \Omega_i^{-1}$ and several interesting features are developing. First, the $\underset{\sim}{B}$ field pulse has broadened considerably. The leading edge of the pulse has been "dragged" out to $x \sim 4r_{Li}$, and the gradients are not as sharp. Second, the laminar electric field has fallen in intensity and is accompanied by a considerable amount of turbulence in the region $0 \lesssim r/r_{Li} \lesssim 2.4$ caused by of the ion-ion streaming. This turbulence causes some momentum exchange between debris and air ions, and thermalization of the particles in this region. Finally, also at this time, a fraction of debris ions have been accelerated to a velocity greater than twice the initial velocity.

Figure 1c shows the system at $t = 0.0874\ \Omega_i^{-1}$. The magnetic pulse continues to broaden and now extends to $x \sim 6r_{Li}$. A laminar electric field still exists at $x \sim 3.6\ r_{Li}$. However, the turbulence in the region $0 <$

$x/r_{Li} \lesssim 3.6$ has subsided since the relative velocity between debris and air ions is small. The ion motion in this region is dominated by the magnetic field and, in effect, is where "Larmor coupling" is taking place. Perhaps the most interesting region is $3.6 < x/r_{Li} < 6.0$. It is clear that debris acceleration and air reflection are continuing. Furthermore, turbulence is developing at the debris-air interface ($x \sim 4.0\ r_{Li}$).

Finally, Fig. 1d shows the system at $t = 0.1542\ \Omega_i^{-1}$. The magnetic pulse is quite broad now, extending out to $x \sim 8.0\ r_{Li}$. Very intense electrostatic turbulence is occurring at the debris-air mix in the region $4.2 \lesssim x/r_{Li} \lesssim 8.2$ which is producing coupling between the ion species and thermalizing the particles. Debris particles have been accelerated up to $V \sim 3V_d$. In the region $2.0 \lesssim x/r_{Li} \lesssim 4.0$ the air ions have a velocity $V \sim 5.0\ V_A$ while the debris ions have a velocity $V \sim 3.0\ V_A$. In this region the momentum coupling is through the magnetic field (Larmor coupling) and the debris and air ions perform gyrations about the magnetic field. Very little turbulence is evident in the electric field, confirming the fact that $\nu^* < \Omega_a$.

Thus, in this simulation it is found that three important processes are affecting coupling, energization, and thermalization: (1) laminar electric fields; (2) turbulent electric fields; and (3) magnetic field pick-up. The laminar fields are most prominent early in the run (Fig. 1a) and cause debris acceleration and air reflection. This is crucial to early time HANE processes since debris ions can be accelerated up to ~ 3 times their initial expansion velocity, and air ions are "picked-up". Turbulent electric fields cause coupling and thermalization of the ion species. In this run they are most effective at the debris-air interface, and ahead of the interface (Figs. 1c and 1d). Finally, "Larmor coupling" is observed within a section of the broad magnetic pulse in Figs. 1c and 1d, i.e., the debris and air ions have rotated about the $\underset{\sim}{B}$ field so that the air ions have a larger $-x$ velocity than that of the debris ($V_{ax} > V_{dx}$). This process supplements any incomplete part of the turbulent coupling and operates on a long time scale.

B. Narrow pulse ($L_B \simeq 0.1\ r_{Li}$)

This simulation is initialized with a magnetic pulse width $L_B \simeq 0.1\ r_{Li}$ and $V_d/V_A = 8$ and $n_d/n_a = 64$. The results are shown in Fig. 2. In Fig. 2a we show the plasma system at $t = 0.0206\ \Omega_i^{-1}$. Already by this time a substantial number of air ions are being reflected from the laminar electric field at $x \sim 1.5\ r_{Li}$. Furthermore, debris ions have been accelerated up to $V \sim 2.5\ V_d$ and extend out to $x \sim 4 r_{Li}$. In this region there is a considerable amount of electrostatic turbulence as seen in the electric field plot. Figure 2b is at $t = 0.0411\ \Omega_i^{-1}$. The magnitude of the turbulence electric fields have increased from the previous time shown and are quite intense at the debris-air interface ($x \sim 3.0\ r_{Li}$). The air ions are being "picked up" because of their turbulence and thermalized. The magnetic field has been dragged out to $x \sim 7.0\ r_{Li}$ by accelerated debris ions. Finally, Figs. 2c and 2d show the ions and fields at $t = 0.0617\ \Omega_i^{-1}$ and $t = 0.0771\ \Omega_i^{-1}$, respectively. The general features are similar to $t = 0.0411$ (Fig. 2b). There are intense turbulent fields at the debris-air interface which transfer momentum from the debris to air ions, and also thermalize the particles. Debris ions extend out to $x \gtrsim 10.0\ r_{Li}$ by $t = 0.0617\ \Omega_i^{-1}$, as well as the $\underset{\sim}{B}$ field and low level turbulence. In this run there is no indication of Larmor coupling. One interesting feature seen in Fig. 2d is the "structuring" of the magnetic pulse. In particular, there is a sharp gradient that has developed at $x \sim 4.8\ r_{Li}$ which produces a laminar electric field. This field acts to energize air ions to such that $V \sim 1.8\ V_d$ at $x \sim 5.0\ r_{Li}$.

IV. DISCUSSION

We have presented the results of simulations of very early time processes (i.e., $t < \Omega_i^{-1}$) using a 1D hybrid code. The purpose of this work has been to elucidate important physical phenomena rather than to perform an actual early time simulation of a HANE. The focus of this study has been primarily on coupling mechanisms; an area that has been somewhat controversial within the DNA community. We have found that there is no "single" coupling mechanism but that several mechanisms can be effective at various times throughout the debris expansion phase. In the first simulation, initialized with a "broad" magnetic pulse, the initial coupling

occurs through laminar electric field at the leading edge of the pulse. Subsequent to this, turbulent coupling occurs at the initial debris-air interface while Larmor coupling occurs within the main body of the magnetic pulse. In the second simulation, initialized with a "narrow" magnetic pulse, the only coupling observed was because of the electric field (laminar and turbulent).

A very important result of this study is the generation of very energetic debris ions. This is caused by the laminar electric field at the leading edge of the magnetic pulse. A fraction of the debris ions can be accelerated up to roughly three times the initial debris expansion velocity (i.e., $V_M \sim 3V_d$). It is well-known that the initial formation of ion debris patches occurs on a time scale faster than that calculated from the initial expansion velocity. Thus, the accelerated debris ions observed in the simulations is consistent with HANE observations.

Finally, this study dramatically highlights the importance of kinetic phenomena for the understanding of early time processes. Kinetic effects such as plasma turbulence, reflected and accelerated ions, and thermalization of the ions are not fluid processes, and cannot be recovered using only MHD codes. Detailed studies are necessary using codes such as the one described in this paper to properly understand the dynamics of early time HANE expansions.

Acknowledgment

This research has been supported by the Defense Nuclear Agency.

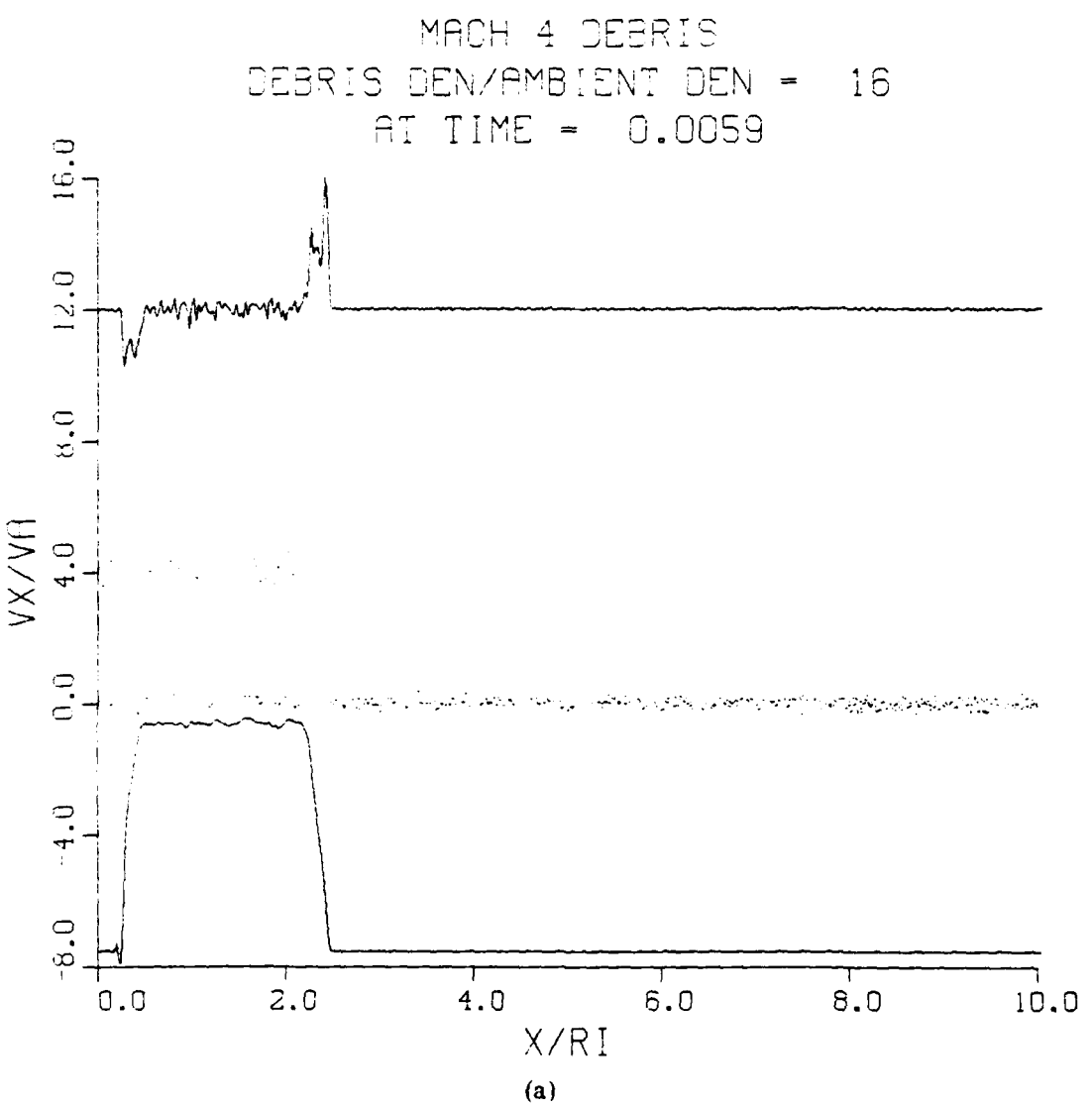

(a)

Fig. 1 — Evolution of the ambient magnetic field (bottom curve), debris and air ions (middle curves/dots), and electric field in x-direction (top curve) as a function of time. The parameters are $M_A = V_d/V_A = 4$, $L_B \sim 2r_{Li}$, and $n_d/n_a = 16$. (a) t = 0.0059 Ω_i^{-1}; (b) t = 0.0386 Ω_i^{-1}; (c) t = 0.0874 Ω_i^{-1}; and (d) t = 0.1342 Ω_i^{-1}.

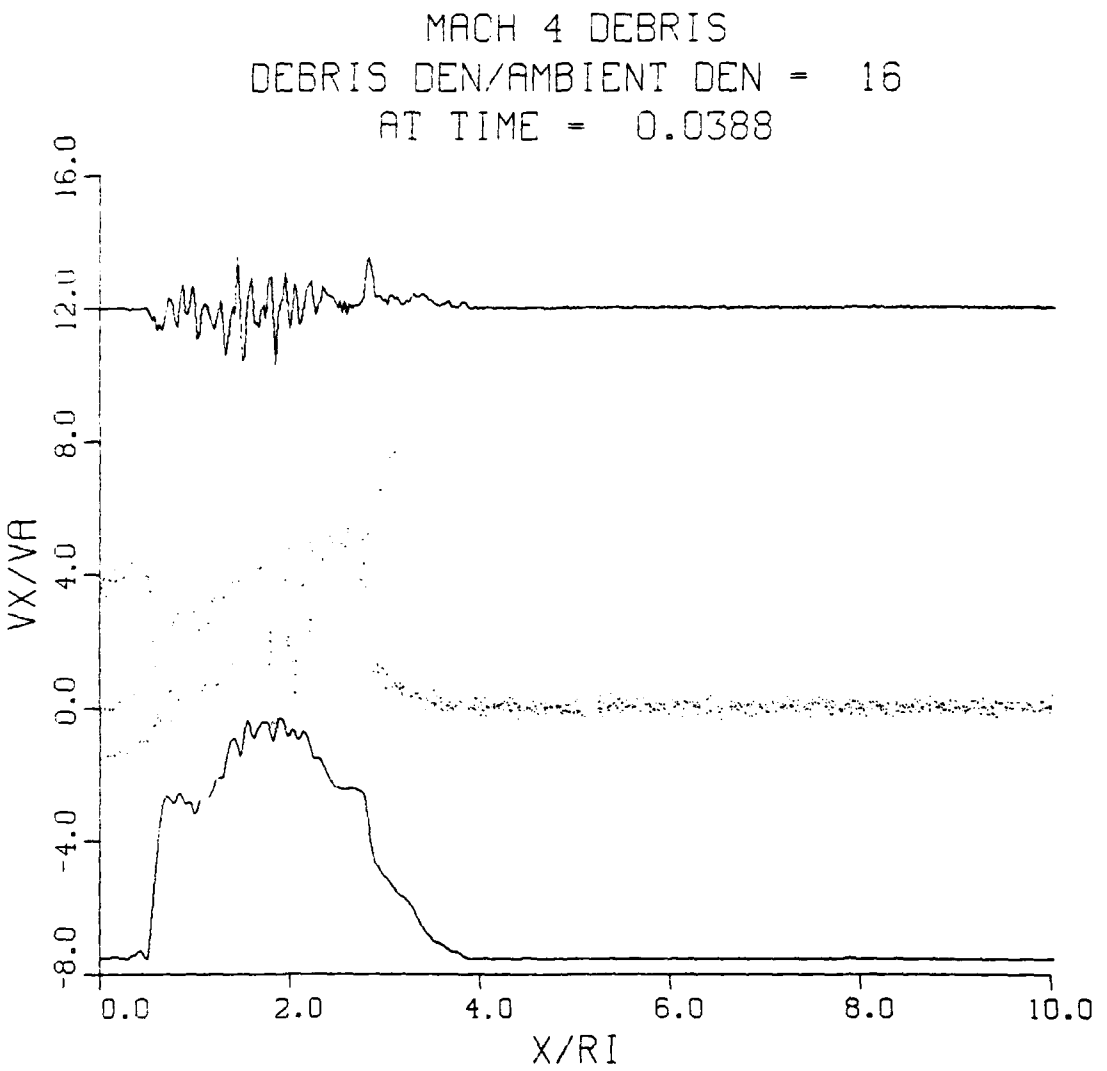

(b)

Fig. 1 (Cont'd) — Evolution of the ambient magnetic field (bottom curve), debris and air ions (middle curves/dots), and electric field in x-direction (top curve) as a function of time. The parameters are $M_A = V_d/V_A = 4$, $L_B \sim 2r_{Li}$, and $n_d/n_a = 16$. (a) $t = 0.0059\ \Omega_i^{-1}$; (b) $t = 0.0386\ \Omega_i^{-1}$; (c) $t = 0.0874\ \Omega_i^{-1}$; and (d) $t = 0.1342\ \Omega_i^{-1}$.

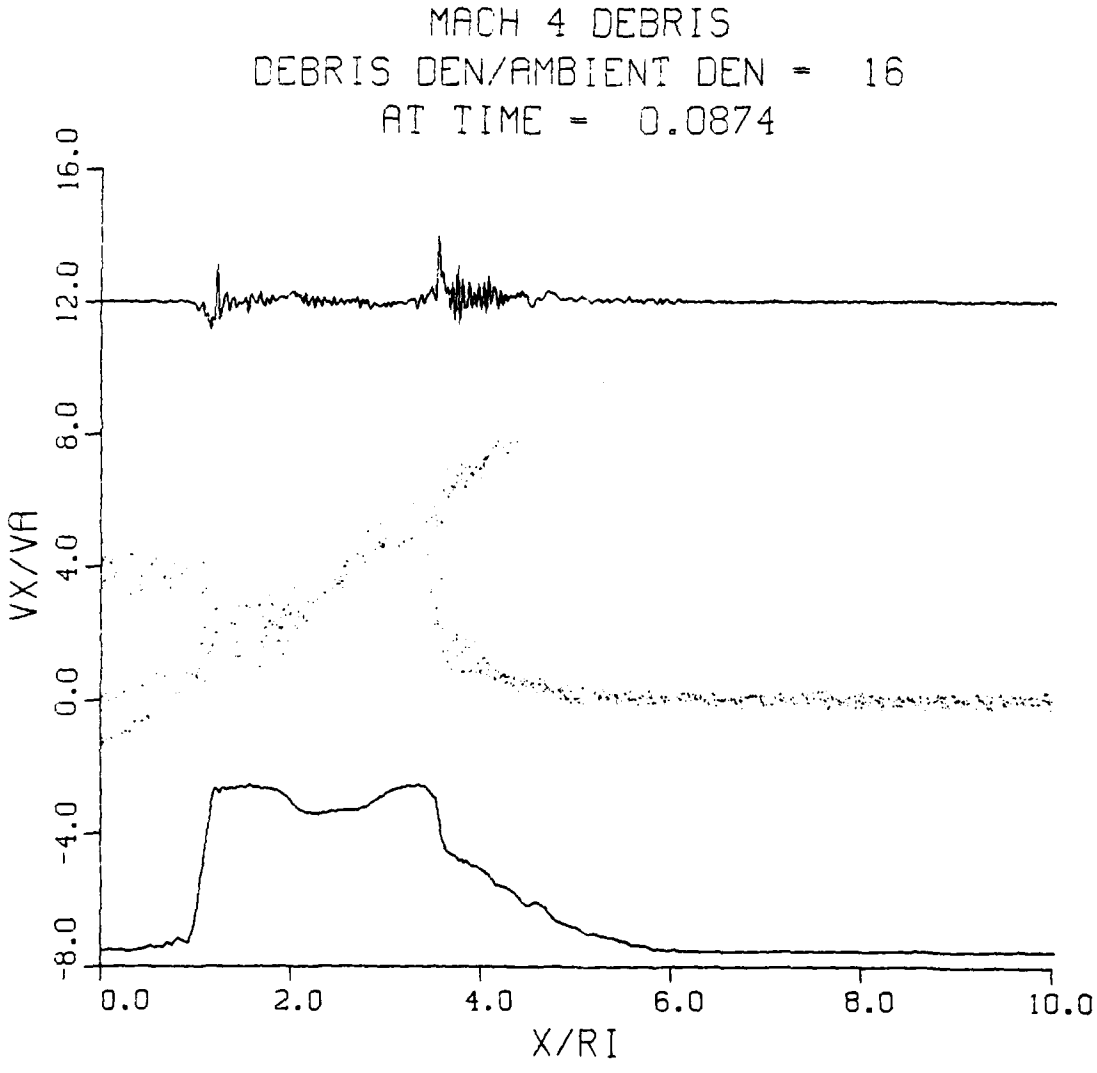

(c)

Fig. 1 (Cont'd) — Evolution of the ambient magnetic field (bottom curve), debris and air ions (middle curves/dots), and electric field in x-direction (top curve) as a function of time. The parameters are $M_A = V_d/V_A = 4$, $L_B \sim 2r_{Li}$, and $n_d/n_a = 16$. (a) t = 0.0059 Ω_i^{-1}; (b) t = 0.0386 Ω_i^{-1}; (c) t = 0.0874 Ω_i^{-1}; and (d) t = 0.1342 Ω_i^{-1}.

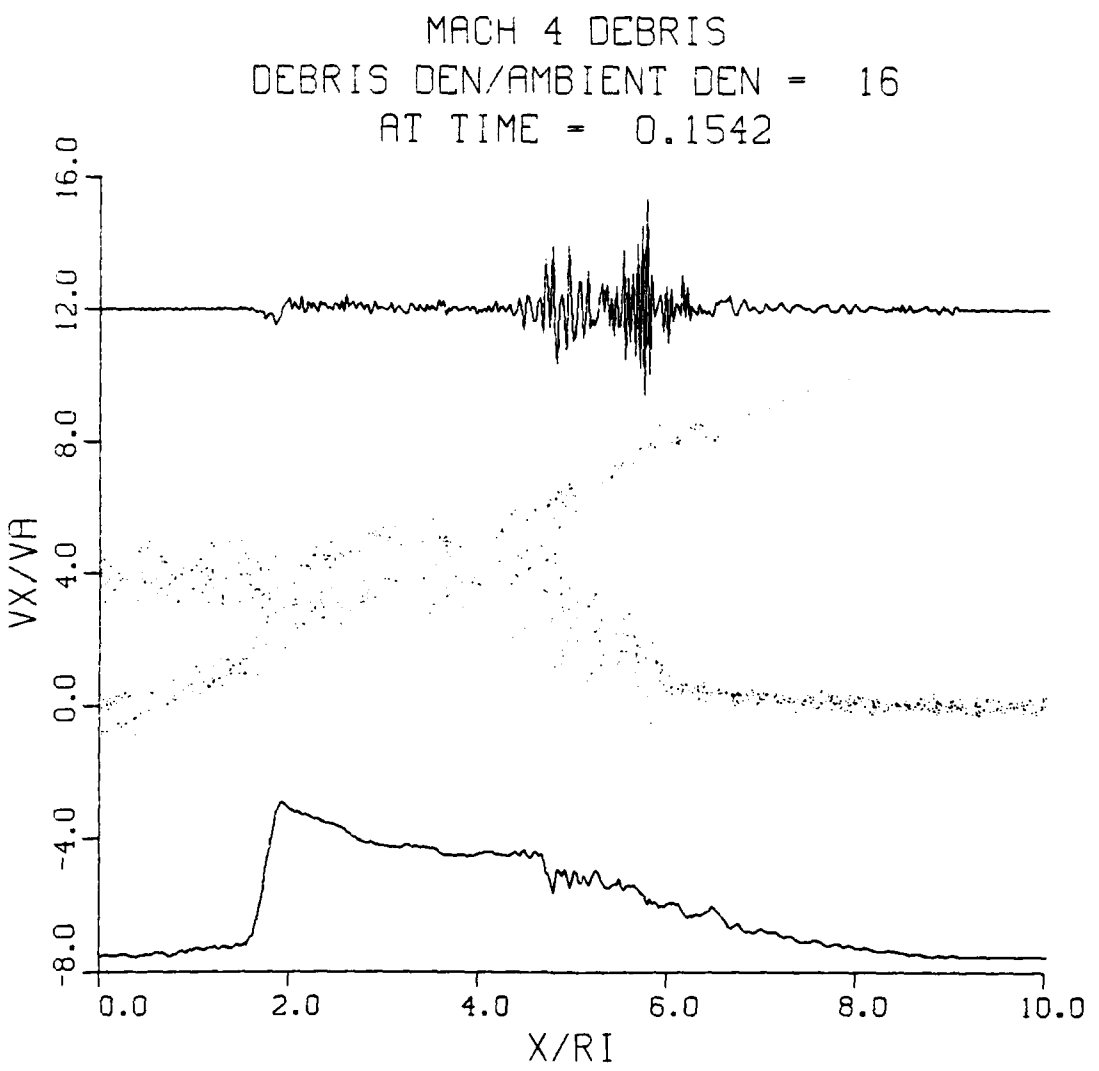

(d)

Fig. 1 (Cont'd) — Evolution of the ambient magnetic field (bottom curve), debris and air ions (middle curves/dots), and electric field in x-direction (top curve) as a function of time. The parameters are $M_A = V_d/V_A = 4$, $L_B \sim 2r_{Li}$, and $n_d/n_a = 16$. (a) t = 0.0059 Ω_i^{-1}; (b) t = 0.0386 Ω_i^{-1}; (c) t = 0.0874 Ω_i^{-1}; and (d) t = 0.1342 Ω_i^{-1}.

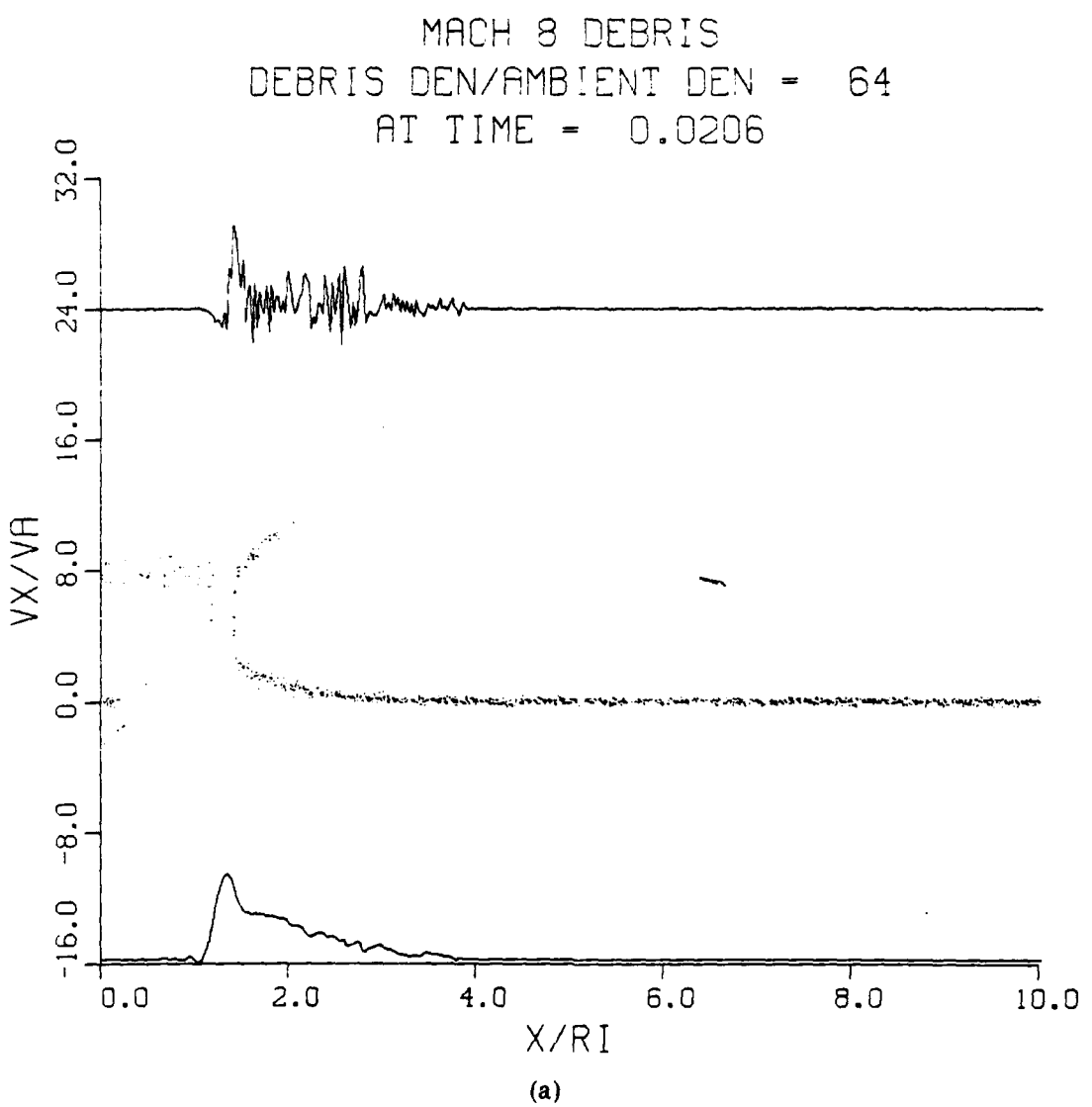

(a)

Fig. 2 — Evolution of quantities described in Figure 1 but with $M_A = V_d/V_A = 8$, $L_B \sim 0.5\ r_{Li}$, and $n_d/n_a = 64$. (a) t = 0.0206 Ω_i^{-1}; (b) t = 0.0411 Ω_i^{-1}; (c) t = 0.0617 Ω_i^{-1}; and (d) t = 0.0771 Ω_i^{-1}.

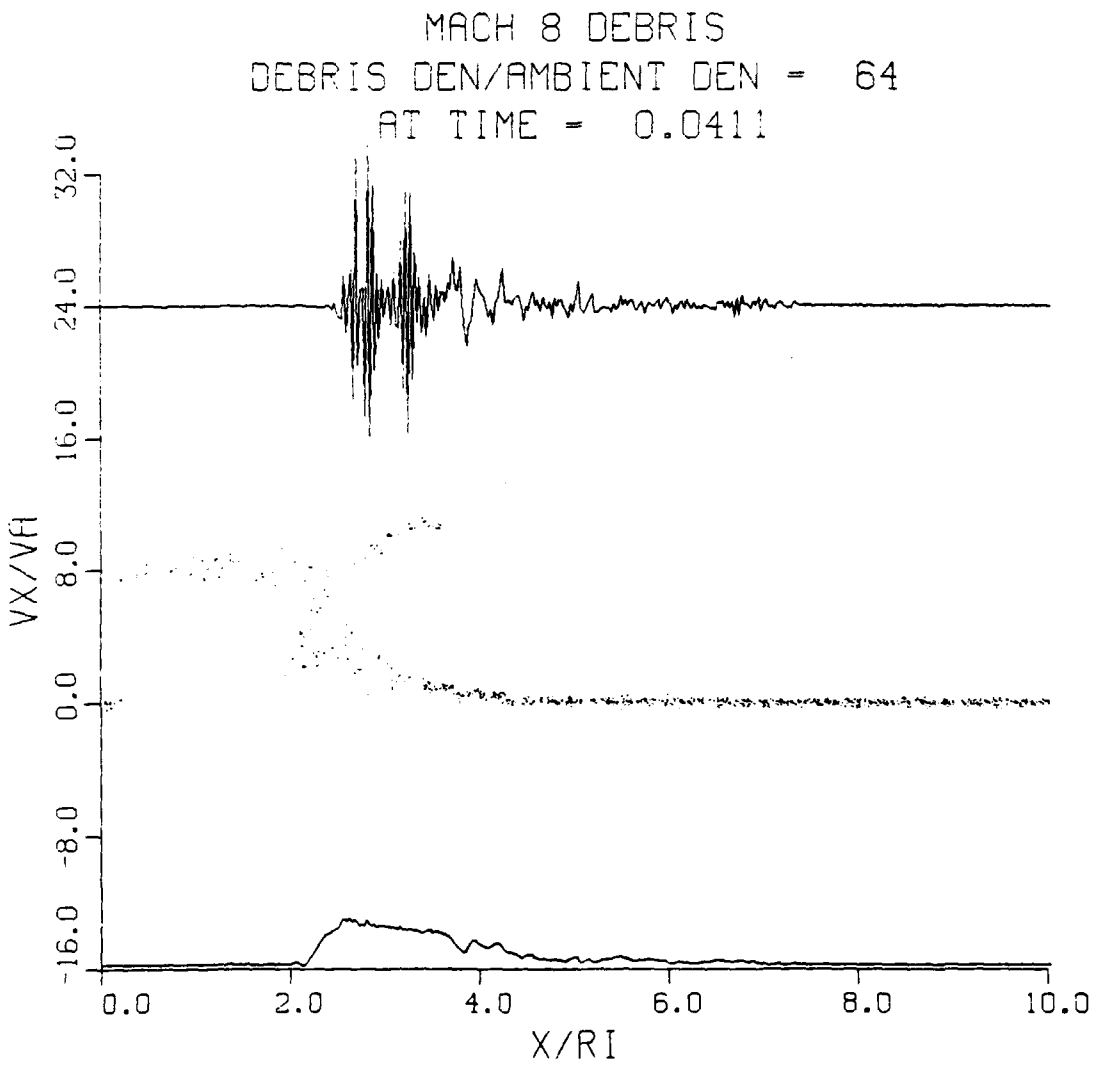

(b)

Fig. 2 (Cont'd) — Evolution of quantities described in Figure 1 but with $M_A = V_d/V_A = 8$, $L_B \sim 0.5\ r_{Li}$, and $n_d/n_a = 64$. (a) t = 0.0206 Ω_i^{-1}; (b) t = 0.0411 Ω_i^{-1}; (c) t = 0.0617 Ω_i^{-1}; and (d) t = 0.0771 Ω_i^{-1}.

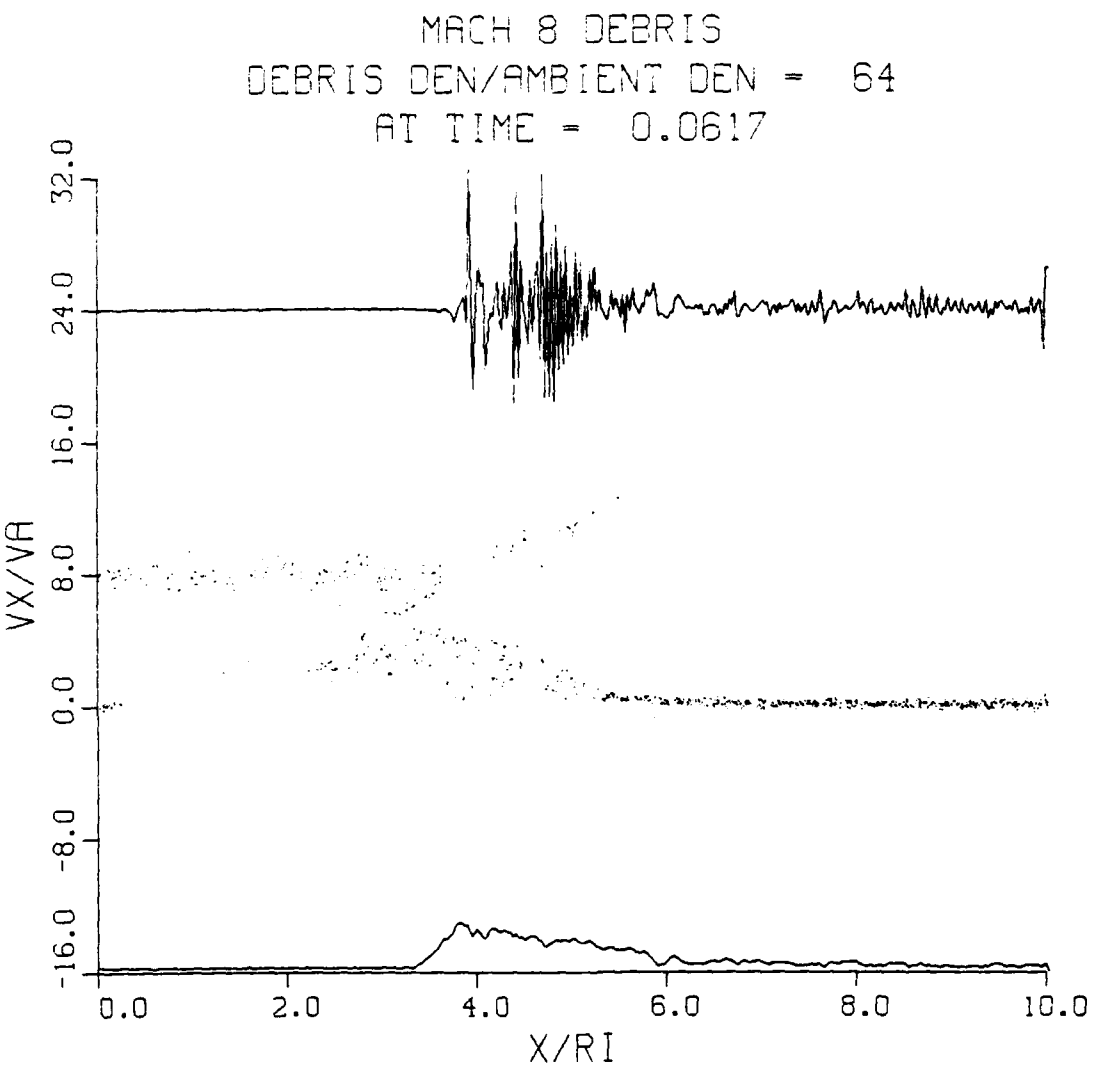

(c)

Fig. 2 (Cont'd) — Evolution of quantities described in Figure 1 but with $M_A = V_d/V_A = 8$, $L_B \sim 0.5\ r_{Li}$, and $n_d/n_a = 64$. (a) $t = 0.0206\ \Omega_i^{-1}$; (b) $t = 0.0411\ \Omega_i^{-1}$; (c) $t = 0.0617\ \Omega_i^{-1}$; and (d) $t = 0.0771\ \Omega_i^{-1}$.

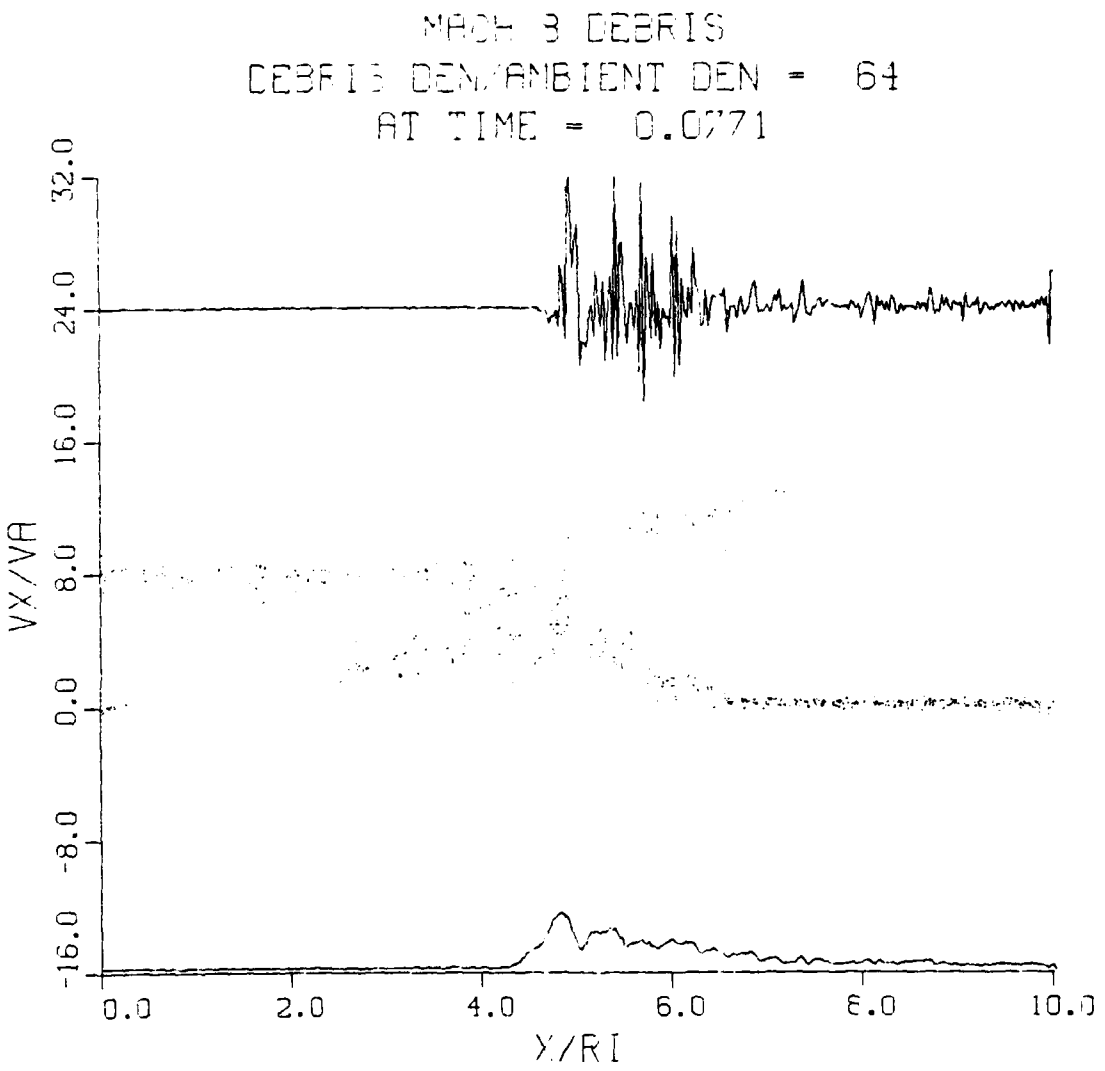

(d)

Fig. 2 (Cont'd) — Evolution of quantities described in Figure 1 but with $M_A = V_d/V_A = 8$, $L_B \sim 0.5\ r_{Li}$, and $n_d/n_a = 64$. (a) $t = 0.0206\ \Omega_i^{-1}$; (b) $t = 0.0411\ \Omega_i^{-1}$; (c) $t = 0.0617\ \Omega_i^{-1}$; and (d) $t = 0.0771\ \Omega_i^{-1}$.

APPENDIX

HYBRID CODE DESCRIPTION

We describe here the numerical details of the hybrid code used in this paper. This description is taken from Winske and Leroy (1983) with minor changes necessary due to the HANE application. Some of the techniques (e.g., particle-in-cell method) are standard and well known, while others (e.g., solution of the field equations) have been applied primarily to fusion-related problems and hence are generally not familiar to the space science community. The discussion is divided into five parts: (A) an overall description of the simulation methods, (B) treatment of the ions, (C) solutions of the field and electron fluid equations, (D) refinements to the basic model, and (E) discussion of the initial and boundary conditions. The methods pertaining to the first four parts are rather general and could thus be applied to any problem where a 'hybrid' (kinetic ion, fluid electron) description is appropriate. Specific adaptation of the method to the HANE study enters primarily through the last topic, the initial and boundary conditions.

A. Overall Description

The simulation method is particle-in-cell (Morse, 1970) with the electrons treated as a fluid (i.e., cell) quantity rather than as discrete particles. The assumption of a massless, charge neutral electron fluid thus eliminates the restriction of time and spatial lengths to he inverse electron plasma frequency and electron Debye length, usually associated with full particle codes. The hybrid models discussed here were originally developed for and extensively applied to dynamical studies of high density pinch experiments by Chodura (1975), Sgro and Nielson (1976) and Hamasaki et al. (1977). These models apply strictly to the case of only one spatial dimension; extension to two dimensions is possible, although nontrivial, as discussed later. Even with only one spatial dimension (which is along the x-axis and thus implies $\partial/\partial y = \partial/\partial z = 0$), all three velocity, magnetic field and electric field components are included. The simulation region has length L, divided into N cells, each of length $\Delta x = L/N$. There is an additional ('ghost') cell at each end of the system, which helps in keeping track of the particles entering and exiting the system and in setting up

the boundary conditions. The cell quantities (i.e., fields, electron fluid properties, ion velocity moments) are specified at the cell centers. Because the restriction to electron spatial and temporal scales has been eliminated, much larger time steps can be used. Typically, the time step (Δt) is limited by the condition that ion gyromotion is well defined and the cell size is constrained by the condition that the fastest ions do not traverse one cell in one time step. The cell size and system length are also chosen to resolve length scales of interest to the problem.

B. Dynamics

The ion component is modeled by a discrete set of particles. The ion distribution is advanced in time by stepping forward each particle in time under the influence of the local, self-consistent Lorentz force. The motion of the ions in a four-dimensional phase space (v_x, v_y, v_z, x) is solved by the particle-in-cell technique, using a second-order-accurate but non-reversible scheme (Nielson and Lewis, 1976). The equations for the ion advance (with superscripts denoting the time level) are:

$$\underset{\sim}{\bar{v}}^{0} = \underset{\sim}{v}^{-1/2} + (h/2)\,\underset{\sim}{E}^{0}$$

$$\underset{\sim}{v}^{1/2} = f\underset{\sim}{v}^{-1/2} + h\left(\underset{\sim}{E}^{0} + g\underset{\sim}{B}^{0} + \frac{\underset{\sim}{\bar{v}}^{0} \times \underset{\sim}{B}}{c} + \underset{\sim}{P}^{0}\right)$$

$$\underset{\sim}{x}^{1} = \underset{\sim}{x}^{0} + \Delta t\ \underset{\sim}{v}^{1/2} \qquad \text{(A1)}$$

where $h = \Delta t\, e/m_i$, $f = 1-(h^2/2)\underset{\sim}{B}^{0} \cdot \underset{\sim}{B}^{0}$, $g = (h/2)(\underset{\sim}{v}^{-1/2} \cdot \underset{\sim}{B}^{0})$, e is the charge and m_i is the mass of the ions. The electric $(\underset{\sim}{E})$ and magnetic fields $(\underset{\sim}{B})$ are evaluated at the particle position $\underset{\sim}{x}^{0}$. $\underset{\sim}{P}$ is a mean friction force, $\underset{\sim}{P} = -e\eta \cdot \underset{\sim}{J}$, exerted by the electrons as a macroscopic force only, $\underset{\sim}{J}$ is the current and η represents a phenomenological anomalous resistivity which gives rise to Ohmic heating, as will be explained later. After all of the ions have been advanced, the ion density (n_i) is updated, by averaging over the positions of all the particles in each cell. The ion mean velocities $(\underset{\sim}{V}_i)$ are also needed at time level 1. The velocities are pushed ahead one half time step,

$$\underset{\sim}{\bar{v}}^{1} = \underset{\sim}{v}^{1/2} + (h/2)\left(\underset{\sim}{E}^{1} + \frac{\underset{\sim}{v}^{1/2} \times \underset{\sim}{B}^{1}}{c} + \underset{\sim}{P}^{1}\right), \qquad \text{(A2)}$$

using the fields at the new particle positions $\underset{\sim}{x}^1$, in order to accumulate the velocity moments $\underset{\sim}{V}_i$.

The assumption of charge neutrality then implies

$$n_e = n_i \equiv n, \tag{A3}$$

and the continuity equation gives

$$\frac{\partial}{\partial t}\left(n_e + n_i\right) = 0 = -\frac{\partial}{\partial x} J_x = -\frac{\partial}{\partial x} en\left(V_{ix} - V_{ex}\right) \tag{A4}$$

or

$$V_{ex} = V_{ix}. \tag{A5}$$

Thus, the electron density and one component of the electron fluid velocity are determined.

C. Field-Fluid Equations

With the assumption of zero electron mass the electron momentum equation reduces to

$$n_e m_e \frac{d\underset{\sim}{V}_e}{dt} = 0 = -en_e\left(\underset{\sim}{E} + \frac{\underset{\sim}{V}_e \times \underset{\sim}{B}}{c}\right) - \frac{\partial}{\partial x} p_e \hat{x} - n_e \underset{\sim}{P} \tag{A6}$$

where p_e is the scalar pressure and $\underset{\sim}{V}_e$ is the velocity of the electron fluid. The transverse (y and z) components of (A6) can be written as Ohm's law

$$\underset{\sim}{J} = \underset{\simeq}{\eta}^{-1} \cdot \left(\underset{\sim}{E} + \frac{\underset{\sim}{V}_e \times \underset{\sim}{B}}{c}\right). \tag{A7}$$

In general, the magnetic field is inclined at some angle with respect to the x axis: $\underset{\sim}{B} = |B|\left(b_x, b_y, b_z\right)$ with $b_x^2 + b_y^2 + b_z^2 = 1$, and if $\sigma_\parallel (\sigma_\perp)$ represents the conductivity parallel (perpendicular) to the magnetic field, the conductivity tensor is (Krall and Trivelpiece, 1973):

$$\underset{\sim}{\sigma} \equiv \underset{\sim}{\epsilon}^{-1} = \begin{matrix} \sigma_1 & \sigma_y & \sigma_z \\ \sigma_y & \sigma_2 & \sigma_x \\ \sigma_z & \sigma_x & \sigma_3 \end{matrix}, \tag{A8}$$

where

$$\sigma_1 = \sigma_\perp + (\sigma_\parallel - \sigma_\perp) b_x b_x$$

$$\sigma_2 = \sigma_\perp + (\sigma_\parallel - \sigma_\perp) b_y b_y$$

$$\sigma_3 = \sigma_\perp + (\sigma_\parallel - \sigma_\perp) b_z b_z$$

$$\sigma_x = (\sigma_\parallel - \sigma_\perp) b_y b_z$$

$$\sigma_y = (\sigma_\parallel - \sigma_\perp) b_x b_z$$

$$\sigma_z = (\sigma_\parallel - \sigma_\perp) b_x b_y .$$

The transverse fields can be expressed in terms of the vector potentials in the usual manner [$\underset{\sim}{B} = \underset{\sim}{\nabla} \times \underset{\sim}{A}$; $\underset{\sim}{E} = -(1/c)(\partial \underset{\sim}{A}/\partial t)$]:

$$\begin{aligned} B_y &= \frac{\partial A_z}{\partial x} \\ B_z &= \frac{\partial A_y}{\partial x} \\ E_y &= -\frac{1}{c}\frac{\partial A_y}{\partial t} \\ E_z &= -\frac{1}{c}\frac{\partial A_z}{\partial t} \end{aligned} \tag{A9}$$

and $\underset{\sim}{\nabla} \cdot \underset{\sim}{B} = 0$ implies

$$B_x = \text{constant}. \tag{A10}$$

(The last field component, E_x, is derived from the x-component of (A6) as will be shown later.)

Neglecting the displacement current, Ampere's law can be expressed

$$\frac{\partial^2 A_y}{\partial x^2} = -\frac{4\pi}{c} J_y$$

$$\frac{\partial^2 A_z}{\partial x^2} = -\frac{4\pi}{c} J_z. \tag{A11}$$

Substituting in Ohm's law (A7) and the definitions of the field components, Eq. (11) becomes a coupled system of equations:

$$\frac{\partial^2 A_y}{\partial x^2} = f_1\left(\frac{\partial A_y}{\partial t}, \frac{\partial A_z}{\partial t}, \frac{\partial A_y}{\partial x}, \frac{\partial A_z}{\partial x}\right)$$

$$\frac{\partial^2 A_z}{\partial x^2} = f_2\left(\frac{\partial A_y}{\partial t}, \frac{\partial A_z}{\partial t}, \frac{\partial A_y}{\partial x}, \frac{\partial A_z}{\partial x}\right). \tag{A12}$$

In order to solve this system a fully implicit, space centered difference scheme is used (Richtmyer and Morton, 1967). If we let $u_j^n = A_y$ at the jth cell position and n-th time level (and $w_j^n = A_z$ in the same way), the left hand side of (A12) is differenced as follows:

$$\frac{\partial^2 A_y}{\partial x^2} = \frac{u_{j+1}^{n+1} + u_{j-1}^{n+1} - 2u_j^{n+1}}{\Delta x^2}, \tag{A13}$$

while on the right hand side

$$\frac{\partial A_y}{\partial t} = \frac{u_j^{n+1} - u_j^n}{\Delta t}$$

and (A14)

$$\frac{\partial A_y}{\partial x} = \frac{u_{j+1}^{n+1} - u_{j-1}^{n+1}}{2\Delta x}.$$

When this is substituted into (A12), the resulting system of equations can be written symbolically as

$$\underset{\sim}{A}_j \cdot \underset{\sim}{X}_{j+1} + \underset{\sim}{B}_j \cdot \underset{\sim}{X}_j + \underset{\sim}{C}_j \cdot \underset{\sim}{X}_{j-1} = \underset{\sim}{D}_j \tag{A15}$$

where

$$\underset{\sim}{X}_j = \begin{matrix} u_j^{n+1} \\ w_j^{n+1} \end{matrix} \tag{A16}$$

and $\underset{\approx}{A}_j$, $\underset{\approx}{B}_j$, and $\underset{\approx}{C}_j$ are 2x2 matrices that depend only on components of $\underset{\approx}{g}$ and $\underset{\sim}{V}_e$ (evaluated at cell j at time level n) and constants, while $\underset{\sim}{D}$ also depends on u_j^n, w_j^n. Thus, all the coefficients $\underset{\approx}{A}$, $\underset{\approx}{B}$, $\underset{\approx}{C}$ and $\underset{\sim}{D}$ are explicitly known. Note that there are N cells in the computation mesh j=1, 2, ... N with ghost cells (j=0 and j=N+1) at each end.

The set of equations (A15) is easily solved. Assuming a solution of the form

$$\underset{\sim}{X}_j = \underset{\approx}{E}_j \cdot \underset{\sim}{X}_{j+1} + \underset{\sim}{F}_j \qquad j = 0,\ 1,\ \ldots\ N \tag{A17}$$

and substituting it into (A15), it then follows that

$$\begin{aligned} \underset{\approx}{E}_j &= -\left[\underset{\approx}{B}_j + \underset{\approx}{C}_j \cdot \underset{\approx}{E}_{j-1}\right]^{-1} \underset{\approx}{A}_j \\ \underset{\sim}{F}_j &= \left[\underset{\approx}{B}_j + \underset{\approx}{C}_j \cdot \underset{\approx}{E}_{j-1}\right]^{-1} \cdot \left[\underset{\sim}{D}_j - \underset{\approx}{C}_j \cdot \underset{\sim}{F}_{j-1}\right] \end{aligned} \tag{A18}$$

Because all the $\underset{\approx}{A}_j$, $\underset{\approx}{B}_j$, $\underset{\approx}{C}_j$ and $\underset{\sim}{D}_j$ are known, if $\underset{\approx}{E}_0$ and $\underset{\sim}{F}_0$ are known (from boundary conditions, as explained later), (A18) can be solved in ascending order to obtain $\underset{\approx}{E}_1$, $\underset{\sim}{F}_1$; $\underset{\approx}{E}_2$, $\underset{\sim}{F}_2$, ..., $\underset{\approx}{E}_N$, $\underset{\sim}{F}_N$. Then if $\underset{\sim}{X}_{n+1}$ can be determined (again from boundary conditions), (A17) can be solved in descending order to obtain $\underset{\sim}{X}_N$, $\underset{\sim}{X}_{N-1}$, ..., $\underset{\sim}{X}_0$.

Once the components of the vector potential are known, the new values of the electric and magnetic field follow from (A9) and the components of the current from (A11), again using the differencing in (A13) and (A14). The transverse components of $\underset{\sim}{V}_e$ are then easily found from the current and the ion velocity moments:

$$V_{ej} = V_{ij} - J_j/en \qquad j = y \text{ or } z. \tag{A19}$$

The last electron fluid quantity to be calculated is the temperature. The electron energy equation can be written as

$$\frac{2}{2}\frac{\partial}{\partial t}\left(n_e T_e\right) + \frac{\partial}{\partial x}\left(\frac{3}{2} n_e T_e V_{ex}\right) + n_e T_e \frac{\partial V_{ex}}{\partial x} = Q. \tag{A20}$$

The source term Q includes resistive heating (ηJ^2) and loss mechanisms, such as thermal conduction or radiation, depending on the application. Letting

$$p_e = n_e T_e, \tag{A21}$$

(A20) can be rewritten in the form (with $\gamma = 5/3$)

$$\left(\frac{\partial}{\partial t} + V_{ex}\frac{\partial}{\partial x}\right)p_e = -\gamma p_e \frac{\partial V_{ex}}{\partial x} + (\gamma-1)Q \tag{A22}$$

The differencing for $\partial p_e/\partial t$ and $\partial V_{ex}/\partial x$ is identical to (A14); for stability reasons "donor cell" differencing is used for the convective term (Richtmyer and Morton, 1967):

$$V_{ex}\frac{\partial p_e}{\partial x} = \frac{V^n_{exj}}{\Delta x} \times \begin{cases} \left(p^{n+1}_{ej} - p^{n+1}_{ej-2}\right) & V_{exj} > 0 \\ \left(p^{n+1}_{ej+1} - p^{n+1}_{ej}\right) & V_{exj} < 0 \end{cases}. \tag{A23}$$

Again, a tridiagonal system is obtained,

$$A_j X_{j+1} + B_j X_j + C_j X_{j-1} = D_j, \tag{A24}$$

except that now all quantities are simple scalars. As before, an assumed solution of the form

$$X_j = E_j X_{j+1} + F_j \tag{A25}$$

leads to

$$E_j = -\left[B_j + C_j E_{j-1}\right]^{-1} A_j$$

$$F_j = [B_j + C_j E_{j-1}]^{-1} [D_j - C_j F_{j-1}]. \tag{A26}$$

Appropriate boundary conditions lead to a determination of E_0, F_0 (and then to all E_j, F_j in ascending order, using (A26)) and X_{N+1} (and thus to all X_j in descending order through (A25)). Since $n_e (= n_i)$ is known, T_e is then obtained from (A21). An alternative to (A22) which is sometimes useful (Sgro, 1978) is to write the energy equation (A20) in terms of the entropy $[S = \ln(p_e n_e^{-\gamma})]$ instead of the pressure.

Finally, the x component of the electron momentum equation (A6) can be solved for E_x:

$$E_x = -\frac{1}{c} (\underset{\sim}{V}_e \times \underset{\sim}{B}_x) - \frac{1}{ne} \frac{\partial p_e}{\partial x} . \tag{A27}$$

This electric field is needed to maintain charge neutrality.

The computation loop through one time step can thus be summarized as follows:

1. Advance the ions one time step and then calculate the ion velocity moments ($n_i = n_e$, $V_{ix} = V_{ex}$, V_{iy}, V_{iz}).
2. Compute the plasma conductivity $\underset{\sim}{g}$, according to some prescription. (The resistivity $\underset{\sim}{\eta}$ is $\underset{\sim}{g}^{-1}$).
3. Solve the coupled equations for A_y, A_z; we can then easily calculate E_y, E_z, B_y, B_z (B_x = constant). From the currents (Ampere's law) and the ion moments calculate the other two electron velocity components, V_{ey} and V_{ez}.
4. The electron temperature is obtained next from the solution of the differenced energy equation.
5. E_x is then calculated from the x-component of the electron momentum equation.
6. Thus, all field and electron fluid components are known and we are ready to move the ions again.

D. Refinements

The simulation scheme described thus far is rather general, the only assumptions being quasineutrality, zero electron mass and one spatial dimension. All of these conditions can be replaced by more appropriate ones, as the physical situation dictates. For example, for the study of low frequency ion waves an adiabatic electron model is more appropriate; such a model has been successfully used by Okuda et al. (1978). In some situations phenomena in the lower hybrid frequency range are of interest. In this case electron inertia effects are non-negligible; they have been included in the one-dimensional model of Liewer (A1976) and the two-dimensional model of Hewett and Nielson (A1978). Two-dimensional simulation models with $m_e = 0$ have been successfully employed by Byers et al. (1978), Hewett (1980) and Harned (1982).

The HANE simulations described in this paper take the conductivity to be constant. A further level of sophistication is to include anomalous processes due to the microphysics, which is occurring on time and distance scales shorter than those resolved in the hybrid model, by means of more complicated transport coefficients. This is done by expressing the conductivity (or resistivity) as a sum of two terms, one representing classical (Spitzer) effects and the other due to anomalous effects arising from microinstabilities due to cross-field currents. Two types of anomalous transport coefficients have been used successfully to model the behavior of laboratory plasmas: one type uses a semi-empirical expression (Chodura, 1975; Sgro and Nielson, 1976), the other is based on a quasilinear analysis of known instabilities (Davidson and Krall, 1977). The transport processes can be further refined to include electron thermal conductivity (Sgro, 1980) and anomalous ion heating (Hamasaki et al., 1977). Multispecies ions can also be included in a straightforward manner (Sgro, 1980; Sgro and Winske, 1981).

E. Initial and Boundary Conditions

In order to simulate the piston formation stage of the HANE problem, appropriate initial and boundary conditions have been implemented in the hybrid code. We assume initially that a dense cool debris plasma flows across the magnetic field into a tenuous stationary air plasma. In this paper, we assume the debris and air to consist of the same ion species. This assumption is not necessary and we are presently investigating the effects of different debris composition. We assume further that there is a magnetic compression of finite width imbedded in the leading edge of the debris stream, formed as a result of the preceding magnetic compression stage of the coupling is simply maintained at the right boundary. Ions of all species are effectively absorbed at the boundaries. The final boundary condition is on the magnetic field which is held constant at the ambient (air) value at both boundaries. The magnetic compression is taken to be proportional to the electron compression. The width of the magnetic compression is an input parameter in the code. Thus initially in the simulation space we establish a debris ion stream extending a finite distance from the left boundary into the uniformly distributed air ions. A step function compression in the magnetic field, narrower than the debris stream, is initialized at the leading edge of the debris. The magnetic field is initially uniform on both sides of the compression. During the simulation runs, debris ions are continuously injected from the left boundary. This is accomplished by re-initializing the debris ion distribution in the left ghost cell each time step.

REFERENCES

Byers, J.A., B.I. Cohen, W.C. Condit, and J.D. Hanson, "Hybrid Simulations of Quasineutral Phenomena in Magnetized Plasma," J Comp. Phys., 27, 363, 1978.

Chodura, R., "Hybrid Fluid-Particle Model of Ion Heating in High-Mach-Number Shock Waves," Nucl. Fusion, 15, 55, 1975.

Davidson, R.C., and N.A. Krall, "Anomalous Transport in High-Temperature Plasmas with Applications to Solenoidal Fusion Systems," Nucl. Fusion, 17, 1313, 1977.

Hamasaki, S., N.A. Krall, C.E. Wagner, and R.N. Byrne, "Effect of Turbulence on Theta Pinch Modeling by Hybrid Numerical Models," Phys. Fluids, 20, 65, 1977

Harned, D.S., "Quasineutral Hybrid Simulation of Macroscopic Plasma Phenomena," J. Comp. Phys., 47, 452, 1982.

Hewett, D.W., "A global method for Solving the Electron-field Equations in a Zero-inertia-electron-hybrid Plasma Simulation Code," J. Comp. Phys., 38, 378, 1980.

Hewett, D.W. and C.W. Nielson, "A Multidimensional Quasineutral Plasma Simulation Model," J. Comp. Phys., 29, 219, 1978.

Krall, N.A. and A.W. Trivelpiece, Principles of Plasma Physics, p. 119, McGraw-Hill, New York 1973.

Liewer, P.C., "Numerical Studies of Ion Reflection in Collisionless Theta-Pinch Implosions Using a Hybrid Vlasov-Fluid Model," Nucl. Fusion, 16, 817, 1976.

Longmire, C.L., "Notes on Debris-Air-Magnetic Interaction," The Rand Corporation Report RM-3386-PR, 1963. AD296597.

Morse, R.L., "Multidimensional Plasma Simulation by the Particle-in-Cell Method," Methods in Computational Physics, Vol.9, Ed. by B. Alder, S. Fernbach and M. Rotenberg, p. 213, Academic Press, NY, 1970.

Nielson, C.W. and H.R. Lewis, "Particle-code Models in the Nonradiative Limit," in Methods in Computational Physics, Vol. 16, edited by J. Killeen, B. Alder, S. Fernbach and M. Rotenberg, p. 367, Academic Press, New York, 1976.

Okuda, H., J.M. Dawson, A.T. Lin and C.C. Lin, "Quasi-neutral Particle Simulation with Application to Ion Wave Propagation," Phys. Fluids, 21, 476, 1978.

Papadopoulos, K., R.C. Davidson, J.M. Dawson, I. Haber, D.A. Hammer, N.A. Krall, and R. Shanny, "Heating of Counterstreaming Ion Beams in an External Magnetic Field," Phys. Fluids, 14, 849, 1971.

Ripin, B.H., J. Grun, S. Kacenjar, E.A. McLean, and J.A. Stamper, "Introduction to the Laser-HANE Experiment and Summary of Low-Pressure Interaction Results," NRL Memo Report 5268, 1984. AD138945.

Sgro, A.G. and C.W.Nielson, "Hybrid Model Studies of Ion Dynamics and Magnetic Field Diffusion During Pinch Implosions," Phys. Fluids, 19, 126, 1976.

Sgro, A.G., "Calculation of the Effects of Incomplete Preionization in High Voltage Theta Pinches," Phys. Fluids, 21, 1410, 1978.

Sgro, A.G., "Simulation of the ZT-S reversed Field Pinch," Phys. Fluids, 23, 1055, 1980.

Sgro, A.G. and D. Winski, "Simulation of the Formation of the PS-1 Spheromak," Phys. Fluids, 24, 1156, 1981.

Winske, D. and M.M. Leroy, "Hybrid Simulation Tech Applied to Earth's Bow Shock," Comp. Simulations of Space Plasmas - Selected Lectures at 1st ISS, D. Reidel, Holland, 1984.

DISTRIBUTION LIST

DEPARTMENT OF DEFENSE

ASSISTANT SECRETARY OF DEFENSE
COMM, CMD, CONT 7 INTELL
WASHINGTON, D.C. 20301

DIRECTOR
COMMAND CONTROL TECHNICAL CENTER
PENTAGON RM BE 685
WASHINGTON, D.C. 20301
01CY ATTN C-650
01CY ATTN C-312 R. MASON

DIRECTOR
DEFENSE ADVANCED RSCH PROJ AGENCY
ARCHITECT BUILDING
1400 WILSON BLVD.
ARLINGTON, VA. 22209
01CY ATTN NUCLEAR
MONITORING RESEARCH
01CY ATTN STRATEGIC TECH OFFICE

DEFENSE COMMUNICATION ENGINEER CENTER
1860 WIEHLE AVENUE
RESTON, VA. 22090
01CY ATTN CODE R410
01CY ATTN CODE R812

DEFENSE TECHNICAL INFORMATION CENTER
CAMERON STATION
ALEXANDRIA, VA. 22314
02CY

DIRECTOR
DEFENSE NUCLEAR AGENCY
WASHINGTON, D.C. 20305
01CY ATTN STVL
04CY ATTN TITL
01CY ATTN DDST
03CY ATTN RAAE

COMMANDER
FIELD COMMAND
DEFENSE NUCLEAR AGENCY
KIRTLAND, AFB, NM 87115
01CY ATTN FCPR

DEFENSE NUCLEAR AGENCY
SAO/DNA
BUILDING 20676
KIRTLAND AFB, NM 87115
01CY D.C. THORNBURG

DIRECTOR
INTERSERVICE NUCLEAR WEAPONS SCHOOL
KIRTLAND AFB, NM 87115
01CY ATTN DOCUMENT CONTROL

JOINT CHIEFS OF STAFF
WASHINGTON, D.C. 20301
01CY ATTN J-3 WWMCCS EVALUATION
OFFICE

DIRECTOR
JOINT STRAT TGT PLANNING STAFF
OFFUTT AFB
OMAHA, NB 68113
01CY ATTN JSTPS/JLKS
01CY ATTN JPST G. GOETZ

CHIEF
LIVERMORE DIVISION FLD COMMAND DNA
DEPARTMENT OF DEFENSE
LAWRENCE LIVERMORE LABORATORY
P.O. BOX 808
LIVERMORE, CA 94550
01CY ATTN FCPRL

COMMANDANT
NATO SCHOOL (SHAPE)
APO NEW YORK 09172
01CY ATTN U.S. DOCUMENTS OFFICER

UNDER SECY OF DEF FOR RSCH & ENGRG
DEPARTMENT OF DEFENSE
WASHINGTON, D.C. 20301
01CY ATTN STRATEGIC & SPACE
SYSTEMS (OS)

WWMCCS SYSTEM ENGINEERING ORG
WASHINGTON, D.C. 20305
01CY ATTN R. CRAWFORD

COMMANDER/DIRECTOR
ATMOSPHERIC SCIENCES LABORATORY
U.S. ARMY ELECTRONICS COMMAND
WHITE SANDS MISSILE RANGE, NM 88002
01CY ATTN DELAS-EO, F. NILES

DIRECTOR
BMD ADVANCED TECH CTR
HUNTSVILLE OFFICE
P.O. BOX 1500
HUNTSVILLE, AL 35807
01CY ATTN ATC-T MELVIN T. CAPPS
01CY ATTN ATC-O W. DAVIES
01CY ATTN ATC-R DON RUSS

PROGRAM MANAGER
BMD PROGRAM OFFICE
5001 EISENHOWER AVENUE
ALEXANDRIA, VA 22333
01CY ATTN DACS-BMT J. SHEA

CHIEF C-E- SERVICES DIVISION
U.S. ARMY COMMUNICATIONS CMD
PENTAGON RM 1B269
WASHINGTON, D.C. 20310
01CY ATTN C- E-SERVICES DIVISION

COMMANDER
FRADCOM TECHNICAL SUPPORT ACTIVITY
DEPARTMENT OF THE ARMY
FORT MONMOUTH, N.J. 07703
01CY ATTN DRSEL-NL-RD H. BENNET
01CY ATTN DRSEL-PL-ENV H. BOMKE
01CY ATTN J.E. QUIGLEY

COMMANDER
U.S. ARMY COMM-ELEC ENGRG INSTAL AGY
FT. HUACHUCA, AZ 85613
01CY ATTN CCC-EMEO GEORGE LANE

COMMANDER
U.S. ARMY FOREIGN SCIENCE & TECH CTR
220 7TH STREET, NE
CHARLOTTESVILLE, VA 22901
01CY ATTN DRXST-SD

COMMANDER
U.S. ARMY MATERIAL DEV & READINESS CMD
5001 EISENHOWER AVENUE
ALEXANDRIA, VA 22333
01CY ATTN DRCLDC J.A. BENDER

COMMANDER
U.S. ARMY NUCLEAR AND CHEMICAL AGENCY
7500 BACKLICK ROAD
BLDG 2073
SPRINGFIELD, VA 22150
01CY ATTN LIBRARY

DIRECTOR
U.S. ARMY BALLISTIC RESEARCH
LABORATORY
ABERDEEN PROVING GROUND, MD 21005
01CY ATTN TECH LIBRARY,
EDWARD BAICY

COMMANDER
U.S. ARMY SATCOM AGENCY
FT. MONMOUTH, NJ 07703
01CY ATTN DOCUMENT CONTROL

COMMANDER
U.S. ARMY MISSILE INTELLIGENCE AGENCY
REDSTONE ARSENAL, AL 35809
01CY ATTN JIM GAMBLE

DIRECTOR
U.S. ARMY TRADOC SYSTEMS ANALYSIS
ACTIVITY
WHITE SANDS MISSILE RANGE, NM 88002
01CY ATTN ATAA-SA
01CY ATTN TCC/F. PAYAN JR.
01CY ATTN ATTA-TAC LTC J. HESSE

COMMANDER
NAVAL ELECTRONIC SYSTEMS COMMAND
WASHINGTON, D.C. 20360
01CY ATTN NAVALEX 034 T. HUGHES
01CY ATTN PME 117
01CY ATTN PME 117-T
01CY ATTN CODE 5011

COMMANDING OFFICER
NAVAL INTELLIGENCE SUPPORT CTR
4301 SUITLAND ROAD, BLDG. 5
WASHINGTON, D.C. 20390
01CY ATTN MR. DUBBIN STIC 12
01CY ATTN NISC-50
01CY ATTN CODE 5404 J. GALET

COMMANDER
NAVAL OCCEAN SYSTEMS CENTER
SAN DIEGO, CA 92152
01CY ATTN J. FERGUSON

NAVAL RESEARCH LABORATORY
WASHINGTON, D.C. 20375
01CY ATTN CODE 4700 S. L. Ossakow
26 CYS IF UNCLASS. 1 CY
IF CLASS)
01CY ATTN CODE 4701 I Vitkovitsky
01CY ATTN CODE 4780 J. Huba (50
CYS IF UNCLASS, 1 CY IF CLASS)
01CY ATTN CODE 7500
01CY ATTN CODE 7550
01CY ATTN CODE 7580
01CY ATTN CODE 7551
01CY ATTN CODE 7555
01CY ATTN CODE 4730 E. MCLEAN
01CY ATTN CODE 4108
01CY ATTN CODE 4730 B. RIPIN
20CY ATTN CODE 2628

COMMANDER
NAVAL SPACE SURVEILLANCE SYSTEM
DAHLGREN, VA 22448
01CY ATTN CAPT J.H. BURTON

OFFICER-IN-CHARGE
NAVAL SURFACE WEAPONS CENTER
WHITE OAK, SILVER SPRING, MD 20910
01CY ATTN CODE F31

DIRECTOR
STRATEGIC SYSTEMS PROJECT OFFICE
DEPARTMENT OF THE NAVY
WASHINGTON, D.C. 20376
01CY ATTN NSP-2141
01CY ATTN NSSP-2722 FRED WIMBERLY

COMMANDER
NAVAL SURFACE WEAPONS CENTER
DAHLGREN LABORATORY
DAHLGREN, VA 22448
01CY ATTN CODE DF-14 R. BUTLER

OFFICER OF NAVAL RESEARCH
ARLINGTON, VA 22217
01CY ATTN CODE 465
01CY ATTN CODE 461
01CY ATTN CODE 402
01CY ATTN CODE 420
01CY ATTN CODE 421

COMMANDER
AEROSPACE DEFENSE COMMAND/DC
DEPARTMENT OF THE AIR FORCE
ENT AFB, CO 80912
01CY ATTN DC MR. LONG

COMMANDER
AEROSPACE DEFENSE COMMAND/XPD
DEPARTMENT OF THE AIR FORCE
ENT AFB, CO 80912
01CY ATTN XPDQQ
01CY ATTN XP

AIR FORCE GEOPHYSICS LABORATORY
HANSCOM AFB, MA 01731
01CY ATTN OPR HAROLD GARDNER
01CY ATTN LKB
KENNETH S.W. CHAMPION
01CY ATTN OPR ALVA T. STAIR
01CY ATTN PHD JURGEN BUCHAU
01CY ATTN D JOHN P. MULLEN

AF WEAPONS LABORATORY
KIRTLAND AFT, NM 87117
01CY ATTN SUL
01CY ATTN CA ARTHUR H. GUENTHER
01CY ATTN NTYCE 1LT. G. KRAJEI

AFTAC
PATRICK AFB, FL 32925
01CY ATTN TN

AIR FORCE AVIONICS LABORATORY
WRIGHT-PATTERSON AFB, OH 45433
01CY ATTN AAD WADE HUNT
01CY ATTN AAD ALLEN JOHNSON

DEPUTY CHIEF OF STAFF
RESEARCH, DEVELOPMENT, & ACQ
DEPARTMENT OF THE AIR FORCE
WASHINGTON, D.C. 20330
01CY ATTN AFRDQ

HEADQUARTERS
ELECTRONIC SYSTEMS DIVISION
DEPARTMENT OF THE AIR FORCE
HANSCOM AFB, MA 01731
01CY ATTN J. DEAS

HEADQUARTERS
ELECTRONIC SYSTEMS DIVISION/YSEA
DEPARTMENT OF THE AIR FORCE
HANSCOM AFB, MA 01732
01CY ATTN YSEA

HEADQUARTERS
ELECTRONIC SYSTEMS DIVISION/DC
DEPARTMENT OF THE AIR FORCE
HANSCOM AFB, MA 01731
01CY ATTN DCKC MAJ J.C. CLARK

COMMANDER
FOREIGN TECHNOLOGY DIVISION, AFSC
WRIGHT-PATTERSON AFB, OH 45433
01CY ATTN NICD LIBRARY
01CY ATTN ETDP B. BALLARD

COMMANDER
ROME AIR DEVELOPMENT CENTER, AFSC
GRIFFISS AFB, NY 13441
01CY ATTN DOC LIBRARY/TSLD
01CY ATTN OCSE V. COYNE

SAMSO/SZ
POST OFFICE BOX 92960
WORLDWAY POSTAL CENTER
LOS ANGELES, CA 90009
(SPACE DEFENSE SYSTEMS)
01CY ATTN SZJ

STRATEGIC AIR COMMAND/XPFS
OFFUTT AFB, NB 68113
01CY ATTN ADWATE MAJ BRUCE BAUER
01CY ATTN NRT
01CY ATTN DOK CHIEF SCIENTIST

SAMSO/SK
P.O. BOX 92960
WORLDWAY POSTAL CENTER
LOS ANGELES, CA 90009
01CY ATTN SKA (SPACE COMM SYSTEMS)
M. CLAVIN

SAMSO/MN
NORTON AFB, CA 92409
(MINUTEMAN)
01CY ATTN MNNL

COMMANDER
ROME AIR DEVELOPMENT CENTER, AFSC
HANSCOM AFB, MA 01731
01CY ATTN EEP A. LORENTZEN

DEPARTMENT OF ENERGY
LIBRARY ROOM G-042
WASHINGTON, D.C. 20545
01CY ATTN DOC CON FOR A. LABOWITZ

DEPARTMENT OF ENERGY
ALBUQUERQUE OPERATIONS OFFICE
P.O. BOX 5400
ALBUQUERQUE, NM 87115
01CY ATTN DOC CON FOR D. SHERWOOD

EG&G, INC.
LOS ALAMOS DIVISION
P.O. BOX 809
LOS ALAMOS, NM 85544
01CY ATTN DOC CON FOR J. BREEDLOVE

UNIVERSITY OF CALIFORNIA
LAWRENCE LIVERMORE LABORATORY
P.O. BOX 808
LIVERMORE, CA 94550
01CY ATTN DOC CON FOR TECH INFO
DEPT
01CY ATTN DOC CON FOR L-389 R. OTT
01CY ATTN DOC CON FOR L-31 R. HAGER

LOS ALAMOS NATIONAL LABORATORY
P.O. BOX 1663
LOS ALAMOS, NM 87545
01CY ATTN DOC CON FOR J. WOLCOTT
01CY ATTN DOC CON FOR R.F. TASCHEK
01CY ATTN DOC CON FOR E. JONES
01CY ATTN DOC CON FOR J. MALIK
01CY ATTN DOC CON FOR R. JEFFRIES
01CY ATTN DOC CON FOR J. ZINN
01CY ATTN DOC CON FOR P. KEATON
01CY ATTN DOC CON FOR D. WESTERVELT
01CY ATTN D. SAPPENFIELD

SANDIA LABORATORIES
P.O. BOX 5800
ALBUQUERQUE, NM 87115
01CY ATTN DOC CON FOR W. BROWN
01CY ATTN DOC CON FOR A.
THORNBROUGH
01CY ATTN DOC CON FOR T. WRIGHT
01CY ATTN DOC CON FOR D. DAHLGREN
01CY ATTN DOC CON FOR 3141
01CY ATTN DOC CON FOR SPACE PROJECT
DIV

SANDIA LABORATORIES
LIVERMORE LABORATORY
P.O. BOX 969
LIVERMORE, CA 94550
01CY ATTN DOC CON FOR B. MURPHEY
01CY ATTN DOC CON FOR T. COOK

OFFICE OF MILITARY APPLICATION
DEPARTMENT OF ENERGY
WASHINGTON, D.C. 20545
01CY ATTN DOC CON DR. YO SONG

OTHER GOVERNMENT

INSTITUTE FOR TELECOM SCIENCES
NATIONAL TELECOMMUNICATIONS & INFO ADMIN
BOULDER, CO 80303
01CY ATTN A. JEAN (UNCLASS ONLY)
01CY ATTN W. UTLAUT
01CY ATTN D. CROMBIE
01CY ATTN L. BERRY

NATIONAL OCEANIC & ATMOSPHERIC ADMIN
ENVIRONMENTAL RESEARCH LABORATORIES
DEPARTMENT OF COMMERCE
BOULDER, CO 80302
01CY ATTN R. GRUBB
01CY ATTN AERONOMY LAB G. REID

DEPARTMENT OF DEFENSE CONTRACTORS

AEROSPACE CORPORATION
P.O. BOX 92957
LOS ANGELES, CA 90009
01CY ATTN I. GARFUNKEL
01CY ATTN T. SALMI
01CY ATTN V. JOSEPHSON
01CY ATTN S. BOWER
01CY ATTN D. OLSEN

ANALYTICAL SYSTEMS ENGINEERING CORP
5 OLD CONCORD ROAD
BURLINGTON, MA 01803
01CY ATTN RADIO SCIENCES

AUSTIN RESEARCH ASSOC., INC.
1901 RUTLAND DRIVE
AUSTIN, TX 78758
01CY ATTN L. SLOAN
01CY ATTN R. THOMPSON

BERKELEY RESEARCH ASSOCIATES, INC.
P.O. BOX 983
BERKELEY, CA 94701
01CY ATTN J. WORKMAN
01CY ATTN C. PRETTIE
01CY ATTN S. BRECHT

BOEING COMPANY, THE
P.O. BOX 3707
SEATTLE, WA 98124
01CY ATTN G. KEISTER
01CY ATTN D. MURRAY
01CY ATTN G. HALL
01CY ATTN J. KENNEY

CHARLES STARK DRAPER LABORATORY, INC.
555 TECHNOLOGY SQUARE
CAMBRIDGE, MA 02139
01CY ATTN D.B. COX
01CY ATTN J.P. GILMORE

COMSAT LABORATORIES
LINTHICUM ROAD
CLARKSBURG, MD 20734
01CY ATTN G. HYDE

CORNELL UNIVERSITY
DEPARTMENT OF ELECTRICAL ENGINEERING
ITHACA, NY 14850
01CY ATTN D.T. FARLEY, JR.

ELECTROSPACE SYSTEMS, INC.
BOX 1359
RICHARDSON, TX 75080
01CY ATTN H. LOGSTON
01CY ATTN SECURITY (PAUL PHILLIPS)

EOS TECHNOLOGIES, INC.
606 Wilshire Blvd.
Santa Monica, Calif 90401
01CY ATTN C.B. GABBARD
01CY ATTN R. LELEVIER

ESL, INC.
495 JAVA DRIVE
SUNNYVALE, CA 94086
01CY ATTN J. ROBERTS
01CY ATTN JAMES MARSHALL

GENERAL ELECTRIC COMPANY
SPACE DIVISION
VALLEY FORGE SPACE CENTER
GODDARD BLVD KING OF PRUSSIA
P.O. BOX 8555
PHILADELPHIA, PA 19101
01CY ATTN M.H. BORTNER
SPACE SCI LAB

GENERAL ELECTRIC COMPANY
P.O. BOX 1122
SYRACUSE, NY 13201
01CY ATTN F. REIBERT

GENERAL ELECTRIC TECH SERVICES CO., INC.
HMES
COURT STREET
SYRACUSE, NY 13201
01CY ATTN G. MILLMAN

GEOPHYSICAL INSTITUTE
UNIVERSITY OF ALASKA
FAIRBANKS, AK 99701
(ALL CLASS ATTN: SECURITY OFFICER)
01CY ATTN T.N. DAVIS (UNCLASS ONLY)
01CY ATTN TECHNICAL LIBRARY
01CY ATTN NEAL BROWN (UNCLASS ONLY)

GTE SYLVANIA, INC.
ELECTRONICS SYSTEMS GRP-EASTERN DIV
77 A STREET
NEEDHAM, MA 02194
01CY ATTN DICK STEINHOF

HSS, INC.
2 ALFRED CIRCLE
BEDFORD, MA 01730
01CY ATTN DONALD HANSEN

ILLINOIS, UNIVERSITY OF
107 COBLE HALL
150 DAVENPORT HOUSE
CHAMPAIGN, IL 61820
(ALL CORRES ATTN DAN MCCLELLAND)
01CY ATTN K. YEH

INSTITUTE FOR DEFENSE ANALYSES
1801 NO. BEAUREGARD STREET
ALEXANDRIA, VA 22311
01CY ATTN J.M. AEIN
01CY ATTN ERNEST BAUER
01CY ATTN HANS WOLFARD
01CY ATTN JOEL BENGSTON

INTL TEL & TELEGRAPH CORPORATION
500 WASHINGTON AVENUE
NUTLEY, NJ 07110
01CY ATTN TECHNICAL LIBRARY

JAYCOR
11011 TORREYANA ROAD
P.O. BOX 85154
SAN DIEGO, CA 92138
01CY ATTN J.L. SPERLING

JOHNS HOPKINS UNIVERSITY
APPLIED PHYSICS LABORATORY
JOHNS HOPKINS ROAD
LAUREL, MD 20810
01CY ATTN DOCUMENT LIBRARIAN
01CY ATTN THOMAS POTEMRA
01CY ATTN JOHN DASSOULAS

KAMAN SCIENCES CORP
P.O. BOX 7463
COLORADO SPRINGS, CO 80933
01CY ATTN T. MEAGHER

KAMAN TEMPO-CENTER FOR ADVANCED STUDIES
816 STATE STREET (P.O DRAWER QQ)
SANTA BARBARA, CA 93102
01CY ATTN DASIAC
01CY ATTN WARREN S. KNAPP
01CY ATTN WILLIAM MCNAMARA
01CY ATTN B. GAMBILL

LINKABIT CORP
10453 ROSELLE
SAN DIEGO, CA 92121
01CY ATTN IRWIN JACOBS

LOCKHEED MISSILES & SPACE CO., INC
P.O. BOX 504
SUNNYVALE, CA 94088
01CY ATTN DEPT 60-12
01CY ATTN D.R. CHURCHILL

LOCKHEED MISSILES & SPACE CO., INC.
3251 HANOVER STREET
PALO ALTO, CA 94304
01CY ATTN MARTIN WALT DEPT 52-12
01CY ATTN W.L. IMHOF DEPT 52-12
01CY ATTN RICHARD G. JOHNSON DEPT 52-12
01CY ATTN J.B. CLADIS DEPT 52-12

MARTIN MARIETTA CORP
ORLANDO DIVISION
P.O. BOX 5837
ORLANDO, FL 32805
01CY ATTN R. HEFFNER

M.I.T. LINCOLN LABORATORY
P.O. BOX 73
LEXINGTON, MA 02173
01CY ATTN DAVID M. TOWLE
01CY ATTN L. LOUGHLIN
01CY ATTN D. CLARK

MCDONNEL DOUGLAS CORPORATION
5301 BOLSA AVENUE
HUNTINGTON BEACH, CA 92647
01CY ATTN N. HARRIS
01CY ATTN J. MOULE
01CY ATTN GEORGE MROZ
01CY ATTN W. OLSON
01CY ATTN R.W. HALPRIN
01CY ATTN TECHNICAL LIBRARY SERVICES

MISSION RESEARCH CORPORATION
735 STATE STREET
SANTA BARBARA, CA 93101
01CY ATTN P. FISCHER
01CY ATTN W.F. CREVIER
01CY ATTN STEVEN L. GUTSCHE
01CY ATTN R. BOGUSCH
01CY ATTN R. HENDRICK
01CY ATTN RALPH KILB
01CY ATTN DAVE SOWLE
01CY ATTN F. FAJEN
01CY ATTN M. SCHEIBE
01CY ATTN CONRAD L. LONGMIRE
01CY ATTN B. WHITE
01CY ATTN R. STAGAT

MISSION RESEARCH CORP.
1720 RANDOLPH ROAD, S.E.
ALBUQUERQUE, NEW MEXICO 87106
01CY R. STELLINGWERF
01CY M. ALME
01CY L. WRIGHT

MITRE CORPORATION, THE
P.O. BOX 208
BEDFORD, MA 01730
01CY ATTN JOHN MORGANSTERN
01CY ATTN G. HARDING
01CY ATTN C.E. CALLAHAN

MITRE CORP
WESTGATE RESEARCH PARK
1820 DOLLY MADISON BLVD
MCLEAN, VA 22101
01CY ATTN W. HALL
01CY ATTN W. FOSTER

PACIFIC-SIERRA RESEARCH CORP
12340 SANTA MONICA BLVD.
LOS ANGELES, CA 90025
01CY ATTN E.C. FIELD, JR.

PENNSYLVANIA STATE UNIVERSITY
IONOSPHERE RESEARCH LAB
318 ELECTRICAL ENGINEERING EAST
UNIVERSITY PARK, PA 16802
(NO CLASS TO THIS ADDRESS)
01CY ATTN IONOSPHERIC RESEARCH LAB

PHOTOMETRICS, INC.
4 ARROW DRIVE
WOBURN, MA 01801
01CY ATTN IRVING L. KOFSKY

PHYSICAL DYNAMICS, INC.
P.O. BOX 3027
BELLEVUE, WA 98009
01CY ATTN E.J. FREMOUW

PHYSICAL DYNAMICS, INC.
P.O. BOX 10367
OAKLAND, CA 94610
ATTN A. THOMSON

R & D ASSOCIATES
P.O. BOX 9695
MARINA DEL REY, CA 90291
01CY ATTN FORREST GILMORE
01CY ATTN WILLIAM B. WRIGHT, JR.
01CY ATTN WILLIAM J. KARZAS
01CY ATTN H. ORY
01CY ATTN C. MACDONALD
01CY ATTN R. TURCO
01CY ATTN L. DeRAND
01CY ATTN W. TSAI

RAND CORPORATION, THE
1700 MAIN STREET
SANTA MONICA, CA 90406
01CY ATTN CULLEN CRAIN
01CY ATTN ED BEDROZIAN

RAYTHEON CO.
528 BOSTON POST ROAD
SUDBURY, MA 01776
01CY ATTN BARBARA ADAMS

RIVERSIDE RESEARCH INSTITUTE
330 WEST 42nd STREET
NEW YORK, NY 10036
01CY ATTN VINCE TRAPANI

SCIENCE APPLICATIONS, INC.
1150 PROSPECT PLAZA
LA JOLLA, CA 92037
01CY ATTN LEWIS M. LINSON
01CY ATTN DANIEL A. HAMLIN
01CY ATTN E. FRIEMAN
01CY ATTN E.A. STRAKER
01CY ATTN CURTIS A. SMITH

SCIENCE APPLICATIONS, INC
1710 GOODRIDGE DR.
MCLEAN, VA 22102
01CY J. COCKAYNE
01CY E. HYMAN

SRI INTERNATIONAL
333 RAVENSWOOD AVENUE
MENLO PARK, CA 94025
01CY ATTN J. CASPER
01CY ATTN DONALD NEILSON
01CY ATTN ALAN BURNS
01CY ATTN G. SMITH
01CY ATTN R. TSUNODA
01CY ATTN DAVID A. JOHNSON
01CY ATTN WALTER G. CHESNUT
01CY ATTN CHARLES L. RINO
01CY ATTN WALTER JAYE
01CY ATTN J. VICKREY
01CY ATTN RAY L. LEADABRAND
01CY ATTN G. CARPENTER
01CY ATTN G. PRICE
01CY ATTN R. LIVINGSTON
01CY ATTN V. GONZALES
01CY ATTN D. MCDANIEL

TECHNOLOGY INTERNATIONAL CORP
75 WIGGINS AVENUE
BEDFORD, MA 01730
01CY ATTN W.P. BOQUIST

TOYON RESEARCH CO.
P.O. Box 6890
SANTA BARBARA, CA 93111
01CY ATTN JOHN ISE, JR.
01CY ATTN JOEL GARBARINO

TRW DEFENSE & SPACE SYS GROUP
ONE SPACE PARK
REDONDO BEACH, CA 90278
01CY ATTN R. K. PLEBUCH
01CY ATTN S. ALTSCHULER
01CY ATTN D. DEE
01CY ATTN D/ STOCKWELL
SNTF/1575

VISIDYNE
SOUTH BEDFORD STREET
BURLINGTON, MASS 01803
01CY ATTN W. REIDY
01CY ATTN J. CARPENTER
01CY ATTN C. HUMPHREY

UNIVERSITY OF PITTSBURGH
PITTSBURGH, PA 15213
01CY ATTN: N. ZABUSKY

DIRECTOR OF RESEARCH
U.S. NAVAL ACADEMY
ANNAPOLIS, MD 21402
02CY

END

FILMED

7-85

DTIC